Accepted Manuscript

Crustal structure across the Teisseyre-Tornquist Zone offshore Poland based on a new refraction/wide-angle reflection profile and potential field modelling

Tomasz Janik, Dariusz Wójcik, Małgorzata Ponikowska, Stanisław Mazur, Tymon Skrzynik, Michał Malinowski, Christian Hübscher

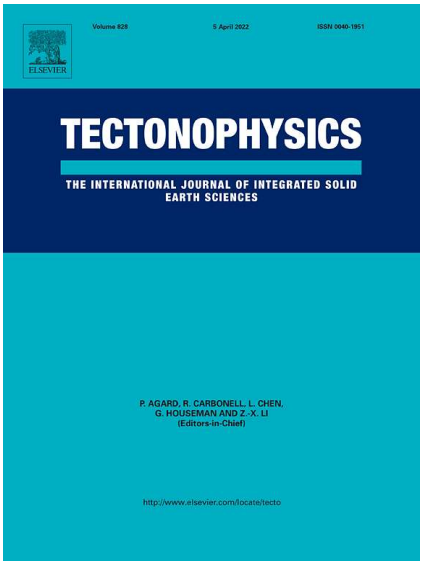

https://doi.org/10.1016/j.tecto.2022.229271
Appeared in: Tectonophysics
Received date: May 01, 2021
Revised date: Feb 09, 2022
Accepted date: Feb 13, 2022
Available online: Feb 22, 2022
Published date: Apr 5, 2022

Please cite this article as: Janik, T., Wójcik, D., Ponikowska, M., Mazur, S., Skrzynik, T., Malinowski, M., Hübscher, C., 2022. Crustal structure across the Teisseyre-Tornquist Zone offshore Poland based on a new refraction/wide-angle reflection profile and potential field modelling, Tectonophysics, 828, doi:10.1016/j.tecto.2022.229271

Crustal structure across the Teisseyre-Tornquist Zone offshore Poland based on a new refraction/wide-angle reflection profile and potential field modelling

Tomasz JANIK[1], Dariusz WÓJCIK[1*], Małgorzata PONIKOWSKA[2], Stanisław MAZUR[2], Tymon SKRZYNIK[1], Michał MALINOWSKI[1,3], Christian HÜBSCHER[4]

[1] Institute of Geophysics, Polish Academy of Sciences, Ks. Janusza 64, PL-01-452 Warszawa, Poland

* (corresponding author) e-mail: dwojcik@igf.edu.pl

[2] Institute of Geological Sciences, Polish Academy of Sciences, Twarda 51/55, PL-00-818 Warszawa, Poland

[3] Geological Survey of Finland (GTK), Vuorimiehentie 5, 02151 Espoo, Finland

[4] Center for Earth System Research and Sustainability, University of Hamburg, Bundesstrasse 55, DE-20146 Hamburg, Germany

Abstract

This paper presents a 230-km long refraction/wide-angle reflection profile that was acquired in the southern Baltic Sea across the Teisseyre-Tornquist Zone (TTZ), the boundary between the East European Craton (EEC) and the West European Platform (WEP). This profile is nearly parallel to the western Polish coast, halfway between Poland and the Danish island of Bornholm. The data acquisition was conducted with 15 ocean bottom seismometers (OBS) and 2 land stations. We applied the trial-and-error iterative ray-tracing technique using all identified seismic phases to derive crustal models by minimizing misfit between calculated and observed P-wave travel-times for individual layers. Final velocity model was further verified by forward potential field modelling, testing various P-wave velocity (V_p) to density relationships. The Moho boundary was inferred at 33-38 km depth, deepening towards the EEC, with the local ~3 km rise in a 40-km-wide zone north of the Caledonian Deformation Front, corresponding to the elevated middle-crust velocities V_p >6.5 km/s. The lower and middle crust are mostly continuous along the BalTec profile with only minor perturbations between the EEC and WEP. Nevertheless, the thickness of these crustal layers is poorly constrained by seismic data along the SW section of the profile. In contrast, the upper crust and sedimentary cover can be subdivided into three domains, corresponding, from the NE to SW, to the EEC, TTZ and WEP, respectively. The EEC is characterised by the flat top of the basement, uniformly inclined towards the SW. The TTZ shows rapid thinning of cratonic upper crust and thickening of sedimentary layer. The WEP reveals, despite limited seismic coverage, a 13-km thick sedimentary overburden. The lateral changes of seismic structure within the upper crust and sedimentary cover along the BalTec profile can be attributed to protracted phases of late Palaeozoic-Mesozoic extension punctuated by the Carboniferous and Late Cretaceous inversion phases.

Keywords

Seismic velocity modelling, Baltic Sea, East European Craton, Moho depth, gravity and magnetic model

1. Introduction

The transition zone from the East European Craton (EEC) to the West European Platform (WEP), conventionally defined as the Teisseyre-Tornquist Zone (TTZ) onshore Poland, is a complex, and not fully understood tectonic feature. It is sometimes considered the craton edge and a Caledonian strike-slip suture representing contact between Baltica and Baltica-derived proximal terranes in the NE and SW, respectively (e.g., Franke, 1994; Dadlez et al., 2005; Narkiewicz et al., 2015; Narkiewicz and Petecki, 2017). However, other researchers postulate continuation of the Baltica lower and middle crust toward the SW beyond the TTZ (e.g., Berthelsen, 1998; Pharaoh, 1999; Lassen et al., 2001; Bayer et al., 2002; Krawczyk et al., 2002). Therefore, in this study, we investigate a continuation of the TTZ in the southern Baltic Sea with the intention to provide further insight into its deep structure and verify the potential presence of a crustal suture aligned with the TTZ. The southern Baltic Sea is of particular interest since the Caledonian Deformation Front (CDF) deviates in that area from the TTZ turning NW-ward (Fig. 1a). Consequently, the TTZ loses its status of a possible tectonic suture and is linked farther north to the Sorgenfrei-Tornquist Zone (STZ; Fig. 1b), an intraplate deformation zone within the EEC (e.g., Thybo et al., 1994; Thybo, 2000).

In order to better constrain the debated crustal and Moho structure across the TTZ south of Bornholm, we use a new wide-angle reflection/refraction (WARR) seismic profile acquired during R/V Maria S. Merian cruise MSM52 in 2016 (Hübscher et al., 2017), hereinafter referred to as the BalTec profile (Fig. 2a). Seismic modelling as well as the analysis and modelling of the gravity and magnetic data are performed along this profile. As a result, we obtain a new 250 km long crustal seismic and gravity models and discuss their tectonic implications. Moreover, we examine contrasting interpretations of the lower crust across the TTZ/STZ with a high-velocity lower crust (V_p>7.0 km/s), typical of underplating, as modelled by Makris and Wang (1994) and a “normal” cratonic lower crust, as modelled by Bleibinhaus et al. (1999).

2. Geological and tectonic setting

The southern Baltic Sea area is in the transition zone between the Fennoscandian Shield as part of the EEC and the WEP. This area is characterised by a mosaic of various geological blocks separated by several fault zones formed throughout the Phanerozoic (Fig. 1b; Liboriussen, 1987; Berthelsen, 1992; Vejbæk et al., 1994; Pharaoh, 1999; Thybo, 2000; van Wees et al., 2000) and it is often defined as the Trans-European Suture Zone (TESZ; Pharaoh, 1999). The most prominent tectonic features are the NW–SE trending STZ and TTZ, crossing the southern Baltic Sea north and south of Bornholm, respectively (Fig. 1a). These zones are characterised by major, often deeply rooted faults (Fig. 1b) that governed subsidence and uplift of major crustal blocks during several tectonic phases in Palaeozoic, Mesozoic

and, locally, also Cenozoic (Dadlez R., 1993; Erlström et al., 1997; Krzywiec et al., 2003; Maystrenko et al., 2005; Al Hseinat and Hübscher, 2017).

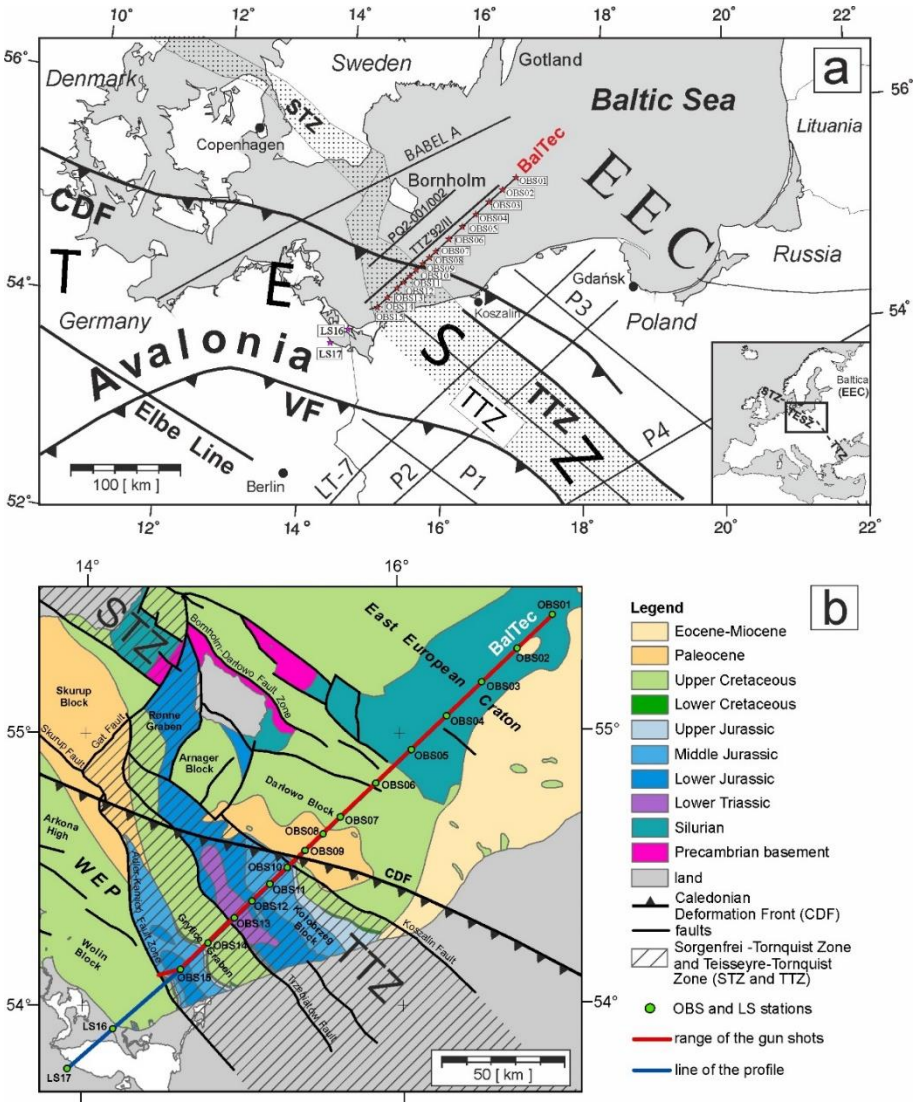

Fig. 1. (a) - Location of the BalTec and other WARR profiles: BABEL A (BABEL Working Group, 1991, 1993), PQ2-001/002 (Bleibinhaus et al., 1999), TTZ'92/II (Makris and Wang, 1994), LT-7'87&91 (Guterch et al., 1994), TTZ-PL'93 (TTZ; Grad et al., 1999), POLONAISE'97 (P1-P4; Guterch et al., 1999) on the background of a simplified tectonic map of the transition zone from the EEC to WEP. Stars and numbers refer to the location of ocean bottom seismometers (OBS) and land stations (LS) along the profile; beginning of the profile corresponds to the first land station (LS17). Abbreviations: CDF – Caledonian Deformation Front; STZ – Sorgenfrei-Tornquist Zone; TESZ – Trans-European Suture Zone; TTZ – Teisseyre-Tornquist Zone; VF – Variscan Front; WEP – West European Platform. (b) - Geological map of the southern Baltic Sea after Kramarska et al. (1999) and Schlüter et al. (1998). Position of main faults and tectonic blocks are modified from Seidel et al. (2018). The position of the Caledonian Deformation Front is after Berthelsen (1992) and Jóźwiak (2013). The coordinate system used in Figures 1b and 2 is WGS 1984 UTM Zone 33N.

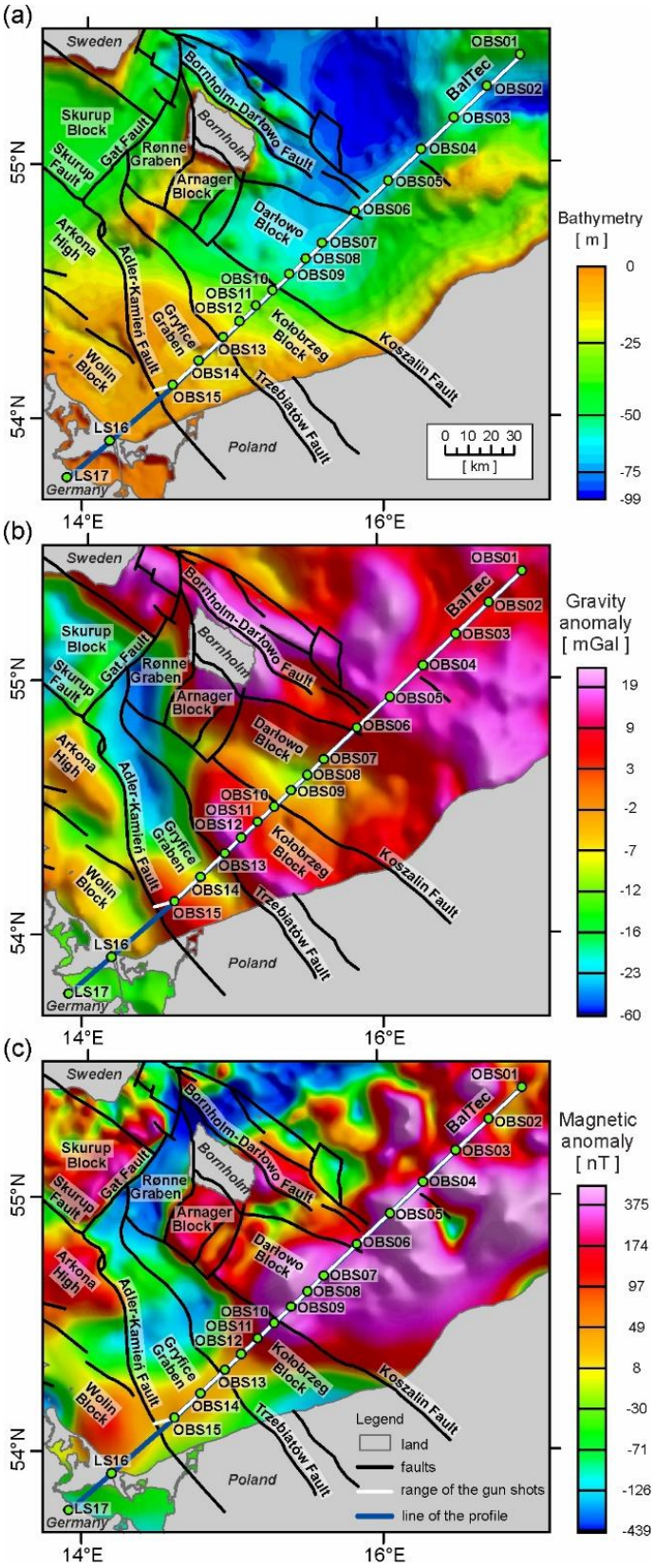

Fig. 2. Bathymetry, gravity and magnetic anomaly maps. Location of main faults and tectonic blocks (modified from Seidel et al., 2018) overlaid on the bathymetry (a), Free Air gravity (b) and Reduced-to-Pole magnetic (c) anomaly maps. Position of the BalTec profile is indicated. Bathymetry, gravity and magnetic data provided by Getech Group plc.

The structure and seismic velocity distribution of the crust and upper mantle in the region have been investigated in a number of multichannel reflection and WARR seismic surveys (e.g., EUGENO-S Working Group, 1988; BABEL Working Group, 1993; Makris and Wang, 1994; Mona Lisa Working Group, 1997; Abramovitz et al., 1998; DEKORP-BASIN Research Group, 1998, 1999; Bleibinhaus et al., 1999; Guterch et al., 1994, 1999; Abramovitz and Thybo, 2000; Grad et al., 1999, 2002). These projects primarily targeted deep crustal structures and the Moho (e.g., Thybo, 1997). The enhanced imaging of sedimentary cover, resting on the Precambrian basement, was provided by the high-resolution deep-reflection seismic data of the BASIN'96 survey (DEKORP-BASIN Research Group, 1998; Meissner and Krawczyk, 1999) and compilation of the BABEL survey (BABEL Working Group, 1993) with industry data (Lassen et al., 2001). Seismic images calibrated by borehole data (Erlström et al., 1997) jointly provide an insight into the deep substratum structure of the southern Baltic Sea and adjacent areas (Krawczyk et al., 2002).

In the Ediacaran, an extensive sandy shelf extended across much of present-day SW Scandinavia with sandstone beds directly overlying Precambrian crystalline basement (Erlström et al., 1997). These are covered by a thin (<100 m) middle Cambrian to Early Ordovician bituminous alum-shale sequence. This succession forms a distinct seismic marker, the O-horizon (e.g., Krawczyk et al., 2002), also visible in the regional seismic data in northern Poland (Krzywiec et al. 2013). The E-W-oriented, N-vergent Caledonian deformation complex of overthrust Ordovician sediments tectonically overlies the EEC basement and its lower Palaeozoic sedimentary cover in the SW Baltic Sea (e.g., Berthelsen, 1992; Katzung et al., 1993; Dallmeyer et al., 1999). The complex bends towards the NW-SE direction farther east, where it approaches the STZ-TTZ and subcrops onshore northern Poland in the so-called Pomeranian Caledonides. The latter area is the only one thus far documented, where Ordovician and Silurian strata are tightly refolded (e.g., Modliński and Podhalańska, 2010). A northward- and eastward-prograding foreland basin developed in front of the Caledonian orogenic wedge during the Late Ordovician-Silurian, onlapping the SW slope of the EEC (e.g., Erlström et al., 1997; Poprawa et al., 1999), and reaching a maximum thickness of nearly 5000 m (Mazur et al., 2018).

During the Devonian and Carboniferous, the area of the southern Baltic Sea was situated close to the Laurussia passive margin and stayed under an extensional regime (Smit et al., 2018). Borehole and reflection seismic data indicate that a system of Devonian to upper Carboniferous half grabens developed owing to reactivation of Caledonian thrusts (Piske et al., 1994; Lassen et al., 2001; Krzywiec et al., 2021). The area was uplifted and deeply eroded after cessation of the Variscan orogeny during the transition to early Permian rifting (McCann, 1996). As a result, the base-Permian discontinuity developed and forms an important seismic regional marker (Vejbæk, 1997). From the early Permian rifting onwards, the area was onlapped by an extensive Zechstein-Mesozoic sedimentary basin system

with the region of the southern Baltic Sea forming a structural link between the Danish Basin and the Mid-Polish Trough (MPT; e.g., Krawczyk et al., 2002; Maystrenko et al., 2008). Late Cretaceous to early Paleogene inversion structures extend from onshore Poland to the Baltic Sea, resulting in an uplift of several kilometres, probably due to the Alpine collision (EUGENO-S Working Group, 1988) and North Atlantic ridge push (Mogensen, 1994). A final Paleogene phase of subsidence, related to the North Sea thermal subsidence, was accompanied by intense salt movements (Scheck and Bayer, 1999).

The precise location and structure of the suture between the pre-Caledonian passive margin of Baltica and East Avalonia is unknown. Its remnants are probably deeply buried beneath the upper Palaeozoic-Mesozoic cover of NW Europe (Tanner and Meissner, 1996). The Precambrian EEC (Baltica) crust has been interpreted to extend SE-wards below the Caledonides and the NE German Basin from seismic data (DEKORP-BASIN Research Group, 1999; Gossler et al., 1999; Krawczyk et al., 1999). At depth, it may extend as far as the Elbe Line beneath the NW German Basin (Berthelsen, 1992; Tanner and Meissner, 1996; Cocks and Fortey, 1998; Bayer et al., 2002; Mazur et al., 2015, 2016; Smit et al., 2016). In consequence, the CDF crossing the southern Baltic Sea should be a thin-skinned feature with a basal detachment probably located along the seismic O-horizon (Krawczyk et al., 2002). In accordance, the Pomeranian Caledonides were interpreted by Mazur et al. (2016) as a thin-skinned fold-and-thrust belt, involving part of the Caledonian foreland basin that was accreted to the advancing Caledonian orogenic wedge. The crustal keel postulated by these authors underneath the Teisseyre-Tornquist Zone, based on gravity modelling, is considered a remnant of a Precambrian suture (Mazur et al., 2016), genetically unrelated to the Caledonian orogeny. However, if the TTZ represents a tectonic suture between East Avalonia and Baltica, coincident with a transverse margin of the latter (Dadlez et al., 2005; Narkiewicz et al., 2015), the Pomeranian Caledonides would be a thick-skinned belt with crustal-scale features potentially recognisable in the BalTec profile.

3. Regional geophysical background

3.1. Potential fields

The regional gravity data for the southern Baltic Sea come from the Getech's Multi-Sat satellite altimetry-derived gravity product. The original data were gridded at a 0.02° resolution corresponding to c. 2.2 km in the y dimension and c. 1.3 km in the x dimension. The gravity anomaly map (Fig. 2b) is a compilation of free air gravity offshore and Bouguer gravity onshore. A complete Bouguer correction was calculated using a rock density of 2.67 g/cm^3. The magnetic data offshore are the marine data (TMI) from the Getech's Baltic Sea compilation. The data were gridded at a 0.01° (~1 km) resolution at a common elevation of 1 km above sea level. The reduction-to-pole (RTP) transform was applied to the magnetic anomaly data.

The Bouguer anomaly map of the study area is dominated by gravity highs in its NE half (Fig. 2b). An important NW-SE oriented anomaly continues from the Swedish coast to Bornholm, coinciding in this area with the STZ (Fig. 1b). South of Bornholm, the same anomaly diverges from the postulated location of the STZ (Fig. 1a) and continues farther in the SE direction, approaching the Polish coast directly NE of the CDF (Fig. 2b). This is the area where a significant basement slope was postulated beneath the Pomeranian Caledonides (Mazur et al., 2016). In the SW half of the area, two narrow positive anomalies extend NNW-SSE offshore Poland (Fig. 2b). They coincide with two anticlines at the NW termination of the Polish Swell that was formed due to the Late Cretaceous-earliest Paleogene inversion of the MPT (Dadlez 1993; Dadlez et al., 1997). The Kamień Anticline to the SW is cored by Lower Jurassic sediments, whereas the Kołobrzeg Anticline to the NE exposes Triassic strata at the base of Quaternary (Fig. 1b). Such a correlation reveals the relationship between gravity anomalies and inversion structures. The Skurup Platform shows an important gravity low that partly merges with another distinct negative anomaly over the Rønne and Gryfice Grabens (Figs. 1b, 2b). The latter anomaly separates the gravity highs associated with the Arkona High and Bornholm Block in the SW and NE, respectively (Figs. 1b, 2b).

The NE part of the study area, corresponding to the EEC, is dominated by quite strong and short-wavelength magnetic anomalies (Fig. 2c) that indicate a relatively shallow magnetic basement. An array of magnetic anomalies reveals ENE-WSW oriented structural grain in the Precambrian basement of the EEC, the trend that is also typical of the onshore part of the EEC (Bogdanova et al., 1996; Mikołajczak et al., 2019). A noticeable feature is a negative anomaly north of Bornholm that overlaps the Rønne Graben but continues farther NE across the STZ (Fig. 2c). A distinct magnetic high coincides with the Arkona High (Figs. 1b, 2c) that is probably associated with a shallow position of the basement. In contrast, a minor magnetic high (<110 nT) in the Wolin Block (Fig. 2c) is possibly related to the presence of the latest Carboniferous-early Permian volcanic rocks (e.g., Breitkreuz et al., 2007) and it is not controlled by a shallow depth to the basement.

3.2. Previous deep seismic studies in the area

Seismic experiments TTZ'92/II and PQ2-001/002 provided relatively short seismic profiles parallel to the BalTec profile (Supplementary Material S1), set between Bornholm and the coast of Poland about 30 km apart (Fig. 1a). The interpretation of TTZ'92/II (Makris and Wang, 1994) assumed a thickening of the upper crust due to compressive forces acting on the NE flank of the STZ. Profile PQ2-001/002 (Bleibinhaus et al., 1999) is consistent with TTZ'92/II down to the middle crust, but interpretations of the lower crust are notably different. The discrepancy concerns not only the over 5 km difference in a Moho depth, but also significant velocity anomalies. Bleibinhaus et al. (1999) suggest P-wave velocity of the lower crust in the range of 6.7-6.8 km/s between the CDF and Bornholm, while Makris and Wang

(1994) postulate a significant increase of the P-wave velocity (V_p=7.0-7.5 km/s) within the Bornholm Block.

Approximately 80 km farther north, between the coast of Sweden and Bornholm, the BABEL A line was situated sub-parallel to the BalTec profile (Fig. 1a). The most recent interpretation of the BABEL A section (Abramovitz et al., 1997) postulates a three-layered crystalline crust with velocities of 6.0-6.2, 6.5-6.6 and 6.9-7.2 km/s in the upper, middle and lower crust, respectively. The Moho depth increases between 35 and 50 km from the SW to NE.

The best quality neighbouring WARR data come from land profiles in Poland. Nearest are two along-strike profiles, TTZ (Grad et al., 1999; Janik et al., 2005) and P3 (Środa et al., 1999), whose NW ends are separated from the SW and central parts of BalTec by ~40 km (TTZ) and ~60 km (P3), respectively. Almost parallel to the BalTec profile are two other profiles, LT-7 (Guterch et al., 1994; Supplementary Material S1) at ~100 km and P2 (Janik et al., 2002) at ~140 km on the SE (Fig. 1a). Compared to BalTec, all these profiles are longer and due to their greater depth range they are more suitable to record the refractions from the upper mantle. The models for the TTZ and P3 profiles show three-layered crust below sediments, with velocities of 5.75-5.95 km/s (consolidated basement, TTZ profile) versus 6.15-6.35 km/s (crystalline basement, P3) in the upper, and 6.55-6.65 and 7.0-7.2 km/s in the middle and lower crust, respectively. The Moho depth was determined at 35-37 km in the parts of the profiles LT-7, P2 and TTZ corresponding to the SW part of BalTec, with a sub-Moho P-wave velocity ~8.25 km/s. The parts of the LT-7 and P3 profiles corresponding to the NE part of BalTec show the Moho at depth 41-43 km.

4. Experiment setup and seismic wavefield

To allow deep crustal studies, a ~230 km long wide-angle-reflection-and-refraction (WARR) profile was set across the TTZ in the South Baltic (Fig. 2a), nearly parallel to the west Polish coast, halfway between Poland and the Danish island of Bornholm. During cruise MSM52, the research vessel MARIA S. MERIAN used an air gun array consisting of 8 GI-guns as a seismic source with a total volume of 32 litres, operating at a pressure of 13.8 MPa (Hübscher et al., 2017). The nominal shot interval was 60 s, however, on the shallow water in the SW portion of the line, shots were fired with a reduced air gun array (4 or 6 guns only) and the shot interval was reduced to 30 or 45 s. The water depth along the profile increases from 16 m in the SW part of the profile to a maximum of 71 m at its NE end (Hübscher et al., 2017; Fig. 2a). The seismic data were recorded by 15 OBS nodes (10 German short period and 5 Polish semi-broadband) and 2 land stations deployed along the profile (see Fig. 1a). The location of record units is shown in Table 1. Data comprised 4 channels for each OBS unit: 3 seismometer vertical components, each recorded with different gain and a hydrophone for the German units, and hydrophone

+ vertical and two horizontal seismometer components for the Polish nodes. Data from land stations comprise vertical and two horizontal components from a semi-broadband seismometer with the response band of 30 s to 100 Hz.

Table 1. Details of seismic stations deployed along the BalTec profile.

STATION	DISTANCE [km]	LONGITUDE	LATITUDE	DEPTH/ ALTITUDE [m]	UNIT
OBS01	271.46	17° 00' 03.78" E	55° 25' 18.36" N	51	German
OBS02	251.50	16° 46' 05.40" E	55° 18' 04.14" N	71	German
OBS03	231.58	16° 32' 08.52" E	55° 10' 52.08" N	54	German
OBS04	211.58	16° 18' 18.06" E	55° 03' 34.32" N	67	Polish
OBS05	191.63	16° 04' 36.60" E	54° 56' 14.46" N	64	German
OBS06	171.64	15° 50' 50.40" E	54° 48' 57.48" N	67	Polish
OBS07	151.66	15° 37' 14.34" E	54° 41' 36.30" N	63	German
OBS08	141.83	15° 30' 39.36" E	54° 37' 55.32" N	63	Polish
OBS09	131.85	15° 23' 49.38" E	54° 34' 17.10" N	56	German
OBS10	121.84	15° 17' 01.44" E	54° 30' 37.20" N	63	Polish
OBS11	111.96	15° 10' 24.66" E	54° 26' 56.04" N	31	German
OBS12	101.94	15° 03' 43.08" E	54° 23' 11.70" N	23	Polish
OBS13	92.02	14° 57' 04.14" E	54° 19' 31.08" N	15	German
OBS14	77.10	14° 47' 10.62" E	54° 13' 55.86" N	15	German
OBS15	61.58	14° 36' 51.00" E	54° 08' 09.30" N	12	German
LS16	24.68	14° 11' 57.90" E	53° 54' 41.50" N	28	Polish
LS17	0.00	13° 54' 51.30" E	53° 46' 03.10" N	19	Polish

In total, 2227 shots were fired. Hydrophone data are of high quality and despite the relatively small source volume, sharp first arrivals of P-wave refractions from sedimentary layers (P_{sed}) and from the upper and middle crust (P_g) are observed at over 120 km offsets for most of the seismic record sections (Ocean Bottom Hydrophones (OBH's) 01-12, with exception of OBH03, Fig. 3). Most of the seismic sections show also clear P-wave reflection from the Moho (P_MP) phases beginning at offsets of 70 km, continuing till the end of the profile. Three sections located at the SW end of the profile have an offset limited to 50-75 km (OBH's 13-15, Fig. 3a, full-length seismic sections are in Supplementary Material S2) due to the very shallow water depth and the increased noise associated, affecting the quality of recording.

Seismic energy was additionally recorded by two land semi-broadband seismic stations (LS16-17) deployed to the SW of the ship's track (Fig. 1). For this reason, the modelled area was extended to the SW, and the origin of the model (0 km) was assumed at LS17. The land stations registered very week energy from the marine sources. Phase correlation, which appear to be the P_MP reflection, is visible against noise only in one of the land seismic sections (LS17, Fig.3a). It is difficult to distinguish other phases.

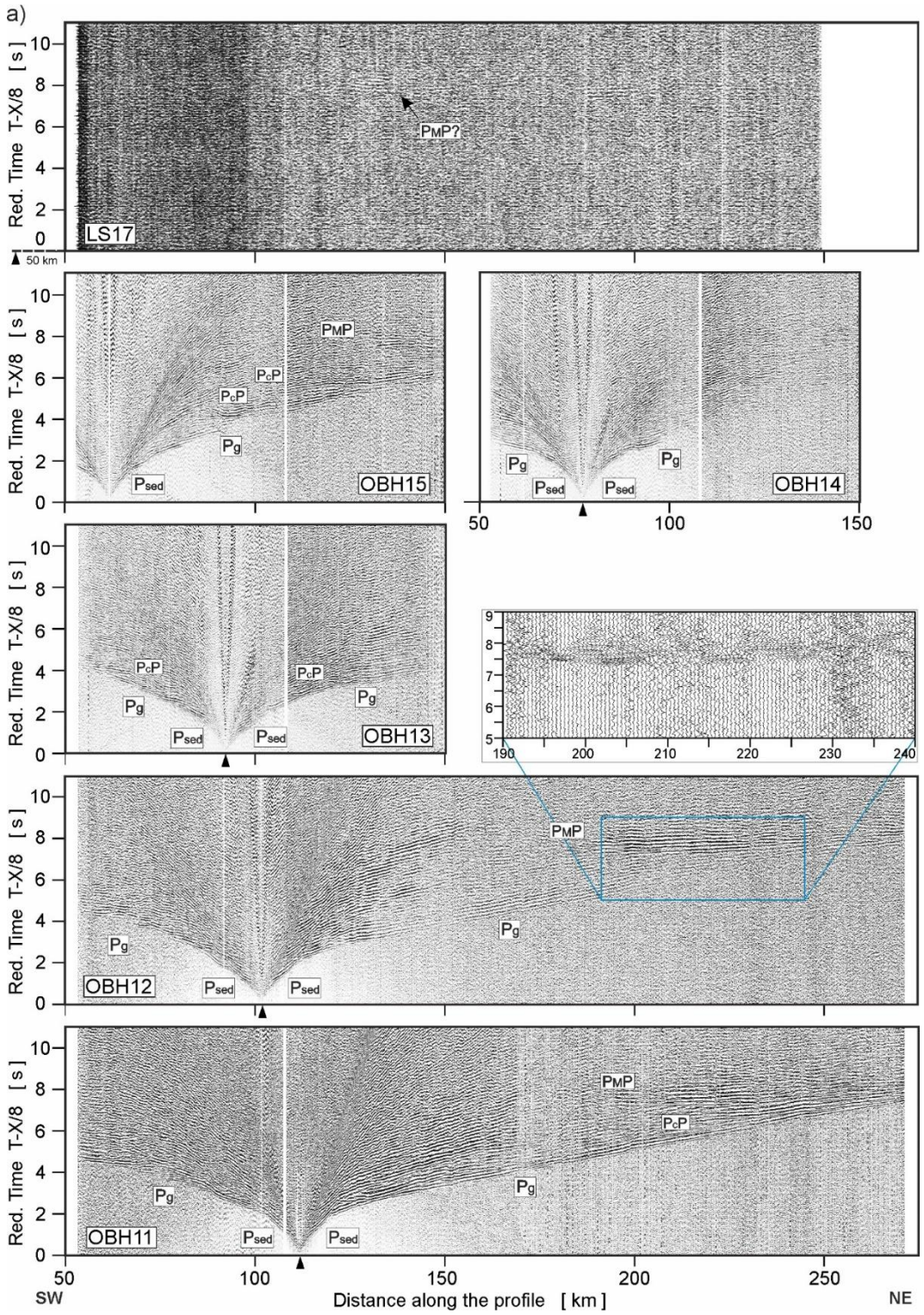

Fig. 3. Examples of trace-normalized, seismic record sections along the BalTec profile for LS17, OBHs 17-11 (a); OBHs 10-06 (b) and OBHs 05-01 (c). A band-pass filter (4-19 Hz) has been applied. At "zooms" examples phases without shade. P_{sed} - P refractions from sedimentary layers; P_g – P refractions from the upper and middle crystalline crust; P_cP – P reflections from the mid-crustal discontinuities, P_MP – P reflections from the Moho boundary; P_n – P refractions from the upper mantle. The reduction velocity is 8.0 km/s.

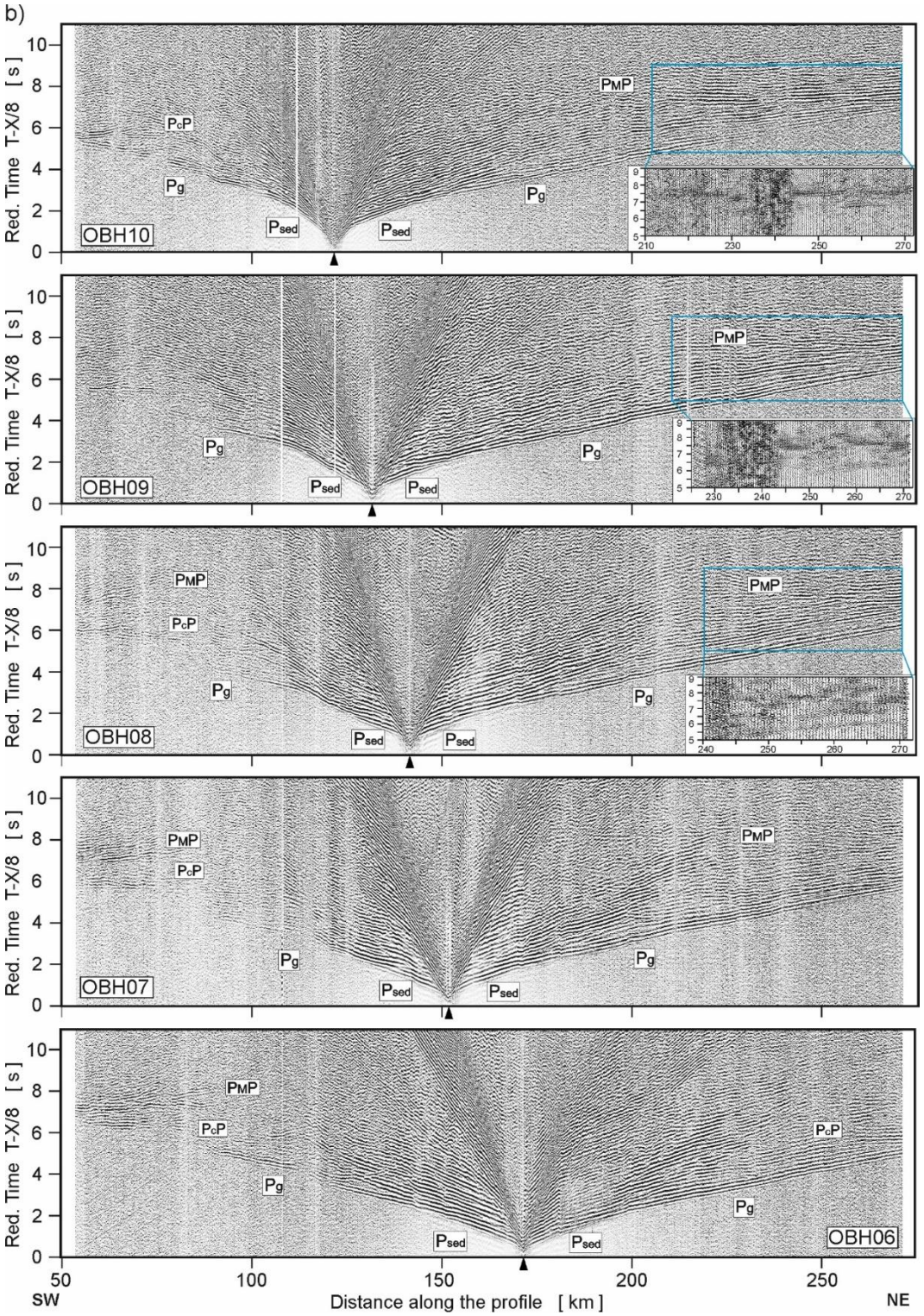

Fig. 3. (continued)

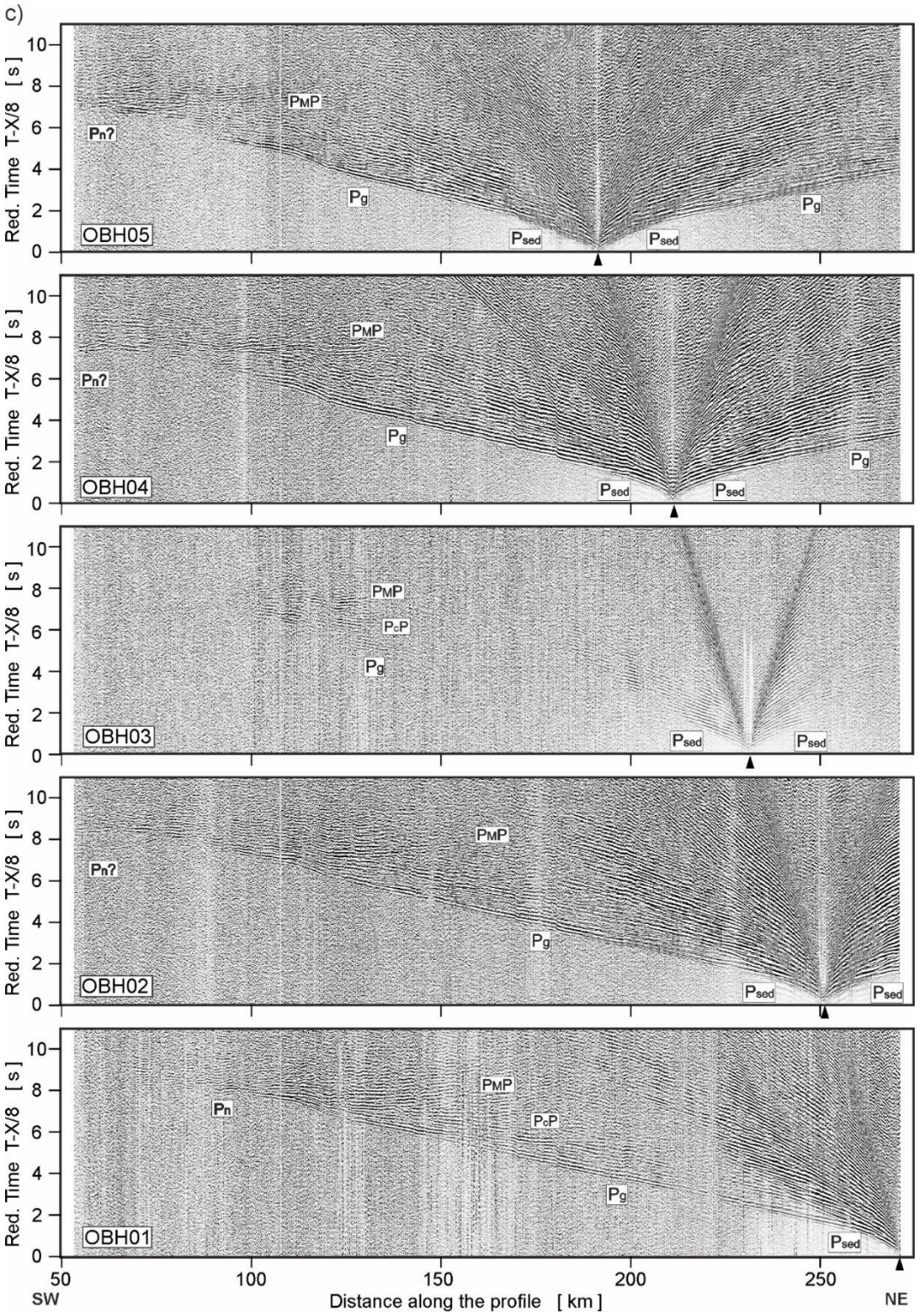

Fig. 3. (continued)

Moving along the profile from SW to NE, significant changes in apparent velocities and offsets are observed for the travel-time arrivals of P_{sed} and P_g phases (Fig. 3). Generally, travel-time arrivals with two apparent velocities, V_p ~2-3 km/s up to 2-4 km and V_p ~3.75-5.5 km/s up to 15-40 km offsets, are

observed on seismic sections up to km 160 of the profile. We interpret them as P_{sed}. Next in the first arrivals, in 2-4 s of a reduced time, the P_g wave with V_p ~5.9-6.1 km/s is visible. For all further sections beyond the profile kilometre 160, the P_g phase begins much earlier, at offsets of 5-15 km and ~1 s of a reduced time. Only a few of the intracrustal reflections (P_cP) can be correlated over a significant distance along the profile, although the crust is strongly reflective and the seismic sections contain additional lower amplitude seismic phases which can be recognized between the P_g and P_MP phases (e.g., OBH15, OBH11, OBH03 and OBH01, Fig. 3). The strongest seismic arrivals observed are reflections from the Moho (P_MP), (e.g., OBH12 at a distance interval of km 175-270, ~7 s reduced time, Fig. 3a). They usually, show a remarkably "ringing" wavefield of ~1 s duration. The nature of the P_MP signal is more clearly shown in the close-ups (Figs. 3a and b). There is a pronounced difference in imaging of the P_MP between the different parts of the profile. In the NW part, the P_MP travel-time arrivals are more continuous along the entire length and have almost the same apparent velocity, close to 8 km/s.

In the SW part of the profile, the P_MP travel-times observed at several sections consist of two intersecting branches. Due to a relatively short length of the profile, the P-wave refraction phase from the mantle (P_n), is generally not observed. Only in the sections for OBH01 (Fig. 3c) between km 90 and 100 of the profile, we can observe the short phase which we may suspect to be P_n. Due to the lack of sufficient observations of mantle refraction (P_n), velocity 8.22 km/s was adopted in the model for uppermost mantle, which is similar to those calculated for the models of the nearest terrestrial profiles, LT-7 (Guterch at al., 1994; see Supplementary Material S1) and TTZ (Grad et al., 1999).

5. Trial-and-error iterative forward modelling

Trial-and-error forward modelling was applied using the 2-D SEIS83 code (Červeny and Psenčik, 1983, 1984). The graphical interface MODEL (Komminaho, 1998) was used to interactively update the model parameters, while a comparison of observed and calculated travel-time arrivals was performed using ZPLOT plotting package (Zelt, 1994). The algorithm implements the ray method for the calculation of ray paths, travel-times and synthetic seismograms. The model consists of layers with smoothly varying velocities, separated by velocity discontinuities. In each layer, the P-wave velocity is parameterized on an arbitrarily defined rectangular grid and interpolated by bicubic splines.

For the preparation of the uppermost part of the initial model, available geological and geophysical data from boreholes located near the profile, as well as information from previous shallow seismic reflection profiles was used (Jaworowski et al., 2010; see Supplementary Material S2). In this way, adding a priori information helped to produce the starting model to be further modified by the trial-and-error ray-tracing procedure. The top layers were then slightly changed if needed to satisfy the data recorded during this study. The model was iteratively modified in order to reach the lowest travel-time misfit. The

simultaneous calculation of synthetic seismograms and qualitative comparison of the amplitudes of synthetic and observed data was performed. This provided additional constraints on the velocity gradients and contrasts at velocity discontinuities. During each iteration, the model was modified in order to reduce the misfit and to ensure similar amplitudes between synthetic and observed data. The iterations proceeded until a satisfactory level of agreement between the observed and calculated travel-times and amplitudes for the main phases was reached and a final model was obtained (Fig. 4). Examples of ray-tracing forward modelling, as well as examples of synthetic seismograms are shown in Figure 5a-g.

5.1. Crustal model and the Moho boundary

The quality of data is reflected in the quality of the model. Good quality registrations (mostly) of P_{sed} and P_g waves make modelling quality of V_p velocities for the upper crust in the offshore part of the profile (km 50-272) much better than onshore. Velocities seem well constrained to the maximum of penetration depth of the modelled refraction waves, ~11-12 km (see Fig. 5). Three zones can be separated in the model (Fig. 4). In the SW part, information about the velocity distribution in the crust is adopted as similar to that from the nearest profiles, TTZ (Grad et al., 1999) and LT-7 (Guterch et al., 1994). The central part represents a transition zone, corresponding to the Teisseyre-Tornquist Zone location between km 65-130, that is characterised by a variable thickness of sedimentary and upper crustal layers. The structure in the NE part of the model shows the flat top of the basement, uniformly inclined to the SW, and a sedimentary cover gradually thickening in the same direction.

Below a thin layer of Cenozoic sediments, the Mesozoic sedimentary sequence has P-wave velocities of 2.4–4.5 km/s to depths of 3-5 km in the SW and central parts and c. 1 km in the NE part of the profile. The upper Palaeozoic strata of a few kilometres thickness have Vp = 5.1–5.8 km/s. There is no clear boundary between the upper and lower Palaeozoic sequences. The Precambrian basement is defined by V_p velocities larger than 6.1 km/s in the NE part of the profile, where its depth increases slowly to ~4 km. The steeper slope is observed between km 130 and 60, where a depth to the crystalline basement top increases SW-ward from 8 to 13 km. However, in the SW part of the profile, the basement is not equally well documented as in the NE. Since the length of the profile is insufficient for recording the refracted wave arrivals from the deeper parts, the ability for determining the velocity in the middle and lower crust is also severely limited. Only a few reflected intracrustal phases have been distinguished. In the modelling phase, different velocities were tested in the lower crust. We firstly tried to apply the solutions from the nearest marine models PQ2-001/002 (Bleibinhaus et al. 1999) and TTZ'92/II (Makris and Wang, 1994). However, it turned out that those solutions did not give a satisfactory level of calculated versus observed travel-time fit and are not applicable to our data. As the P_MP wave was recorded on the majority of seismic sections, the modelling was focused on the best matching of

theoretical travel-times to these phases, with the assumed velocities for individual model bodies in the lower crust for SW, central and NE parts of the model, respectively. Finally, among the tested 2D models, the following four sets of lower crustal velocities were chosen: V_p = 6.75-6.8, 6.6, 7.15 km/s (Model 1); V_p = 7.15, 7.06, 7.15 km/s (Model 2); unified V_p = 7.12-7.13 km/s (Model 3); and V_p = 7.12, 7.12, 7.16 km/s (Model 4); the last model is shown in Figure 4. Models 1, 2 and 3 are attached in Supplementary Material S2. An additional criterion important for modelling is a comparison between the travel-time arrivals for only one visible wave which we interpret as P_MP on the LS17 section.

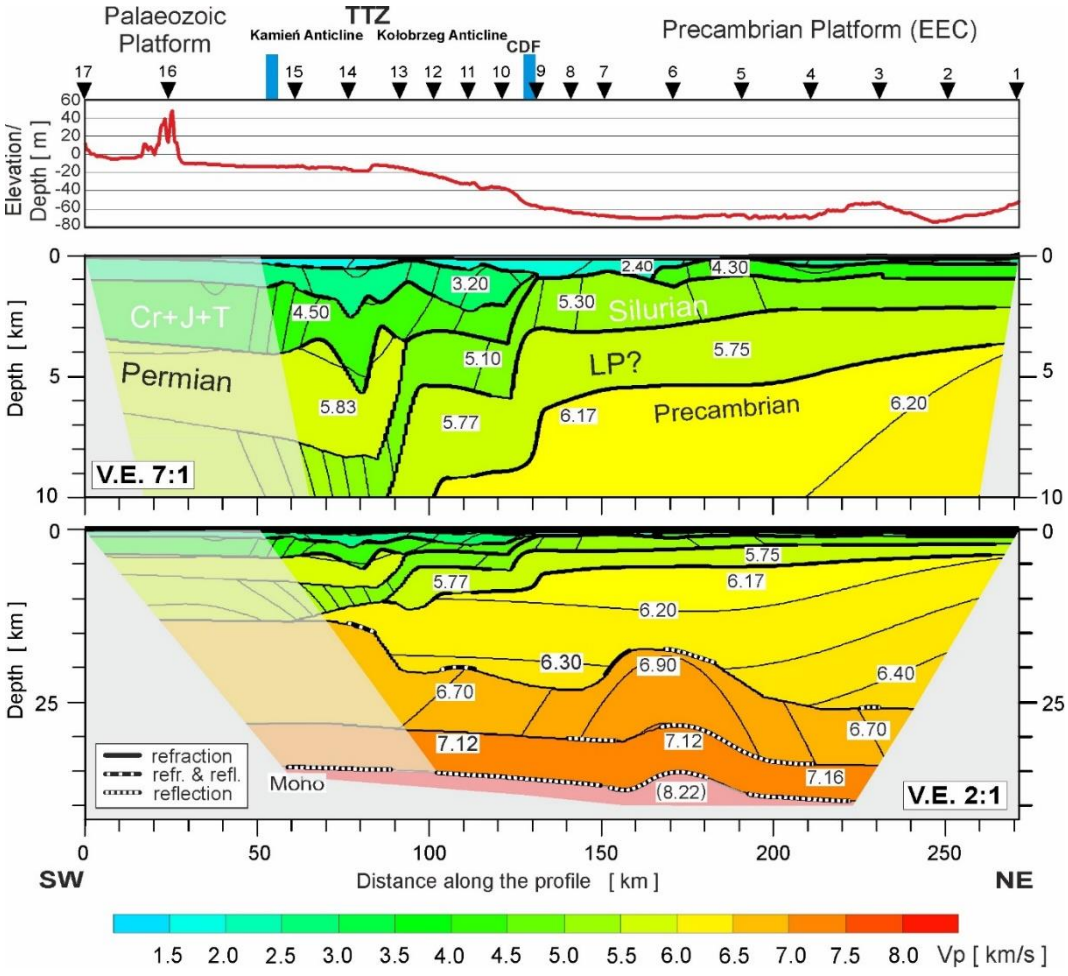

Fig. 4. Two-dimensional models of seismic P- and S-wave velocity in the crust and upper mantle derived by forward ray-tracing modelling using the SEIS83 package (Červený and Pšenčík, 1984) along the BalTec profile. Thick, black solid and dashed lines represent major velocity discontinuities (interfaces). Only those parts of the discontinuities that have been constrained by reflected or refracted arrivals of P-waves are shown. Thin lines represent velocity isolines with values in km/s shown in white boxes. The position of tectonic units is indicated. Black triangles show positions of receiver points. Abbreviations as in Figure 1. Vertical exaggerations are 7:1 for upper part of the model, and 2:1 for the whole model. A semi-transparent polygon represents the part of the model that is not sufficiently covered by seismic rays.

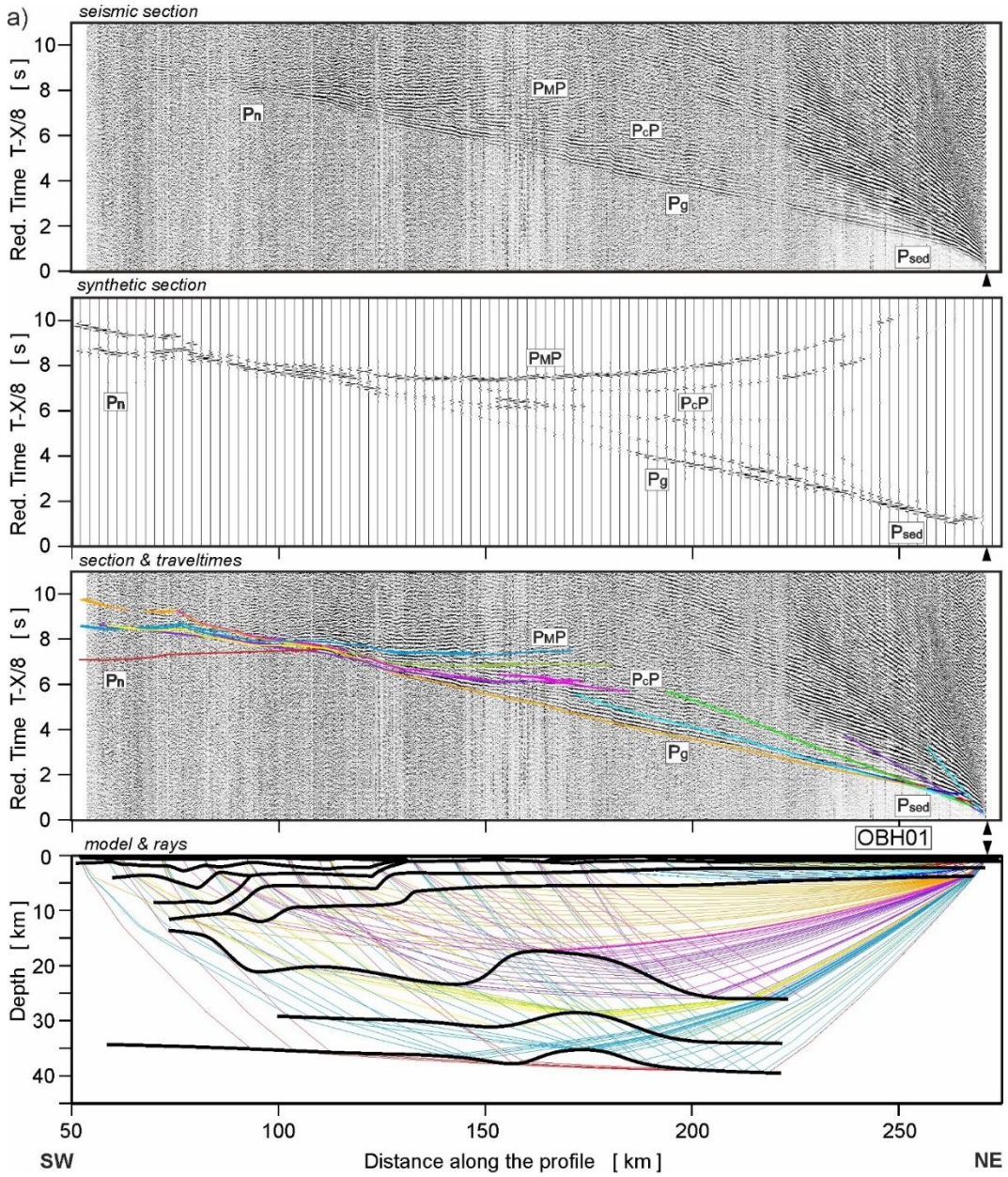

Fig. 5. Examples of the results of the modelling of the P-waves calculated for the final crustal model (Figure 4) for OBH01 a), OBH04 b), OBH08 c), OBH10 d), OBH11 e), OBH15 f), LS17 g) from the BalTec profile. Top – Ray synthetic seismograms using SEIS83 package (Červeny and Psenčik, 1984). Middle – Amplitude-normalized seismic record sections and theoretical travel-times. Bottom – Ray diagram of selected rays. Abbreviations of seismic phases as in Figure 3.

Based on the calculated synthetic section (Fig. 5g), calculations of the theoretical amplitudes of the P_MP and P_n waves for the continental crust models (Guterch, 1970), as well as our experience with constructing seismic models, we assume that the pulses visible in the LS17 section are P_MP pulses (the strongest). On the other hand, much weaker P_n travel-time arrivals are invisible against the background noise.

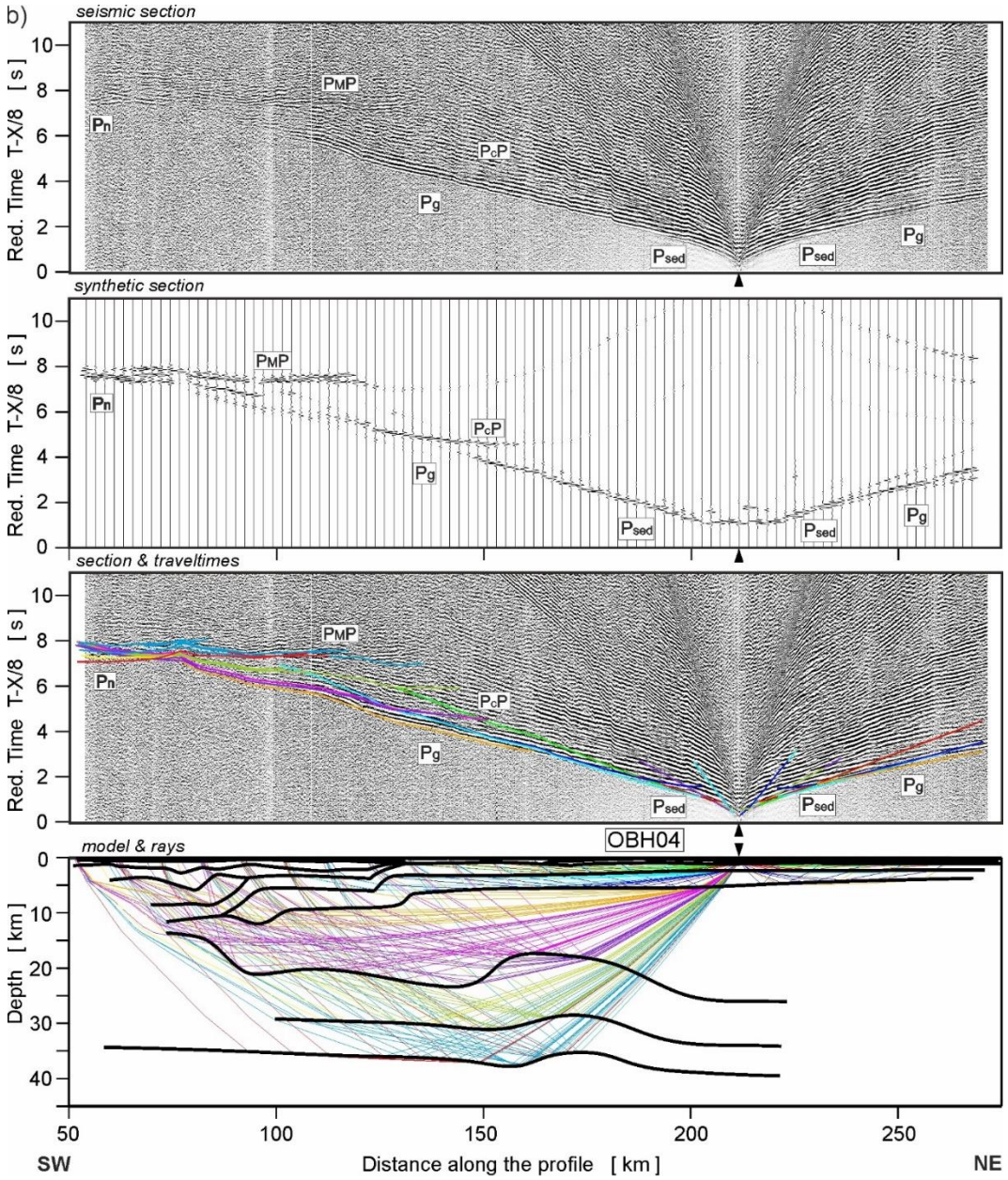

Fig. 5. (continued)

Based on this assumption, we can argue that Model 1 with velocities $V_p < 7$ km/s shows the P_n travel-time arrivals in place of the interpreted P_MP wave, which results in the delay of P_MP theoretical travel-time by 1.0 s at most. Figure 5 in Supplementary Material S2 illustrates this discrepancy by comparing the theoretical travel-times calculated for Models 1 and 4, the latter being our preferred model. This seems to exclude the solution from Model 1. Then two variants of the models, quite complex Model 2 and simplified Model 3, with higher velocities ($V_p > 7$ km/s) in the middle-lower part of the model were tested. They gave a much better agreement for the P_MP wave for the LS17 section, but still there was an inconsistency of the P_MP arrivals on sections from other stations (see Table 2).

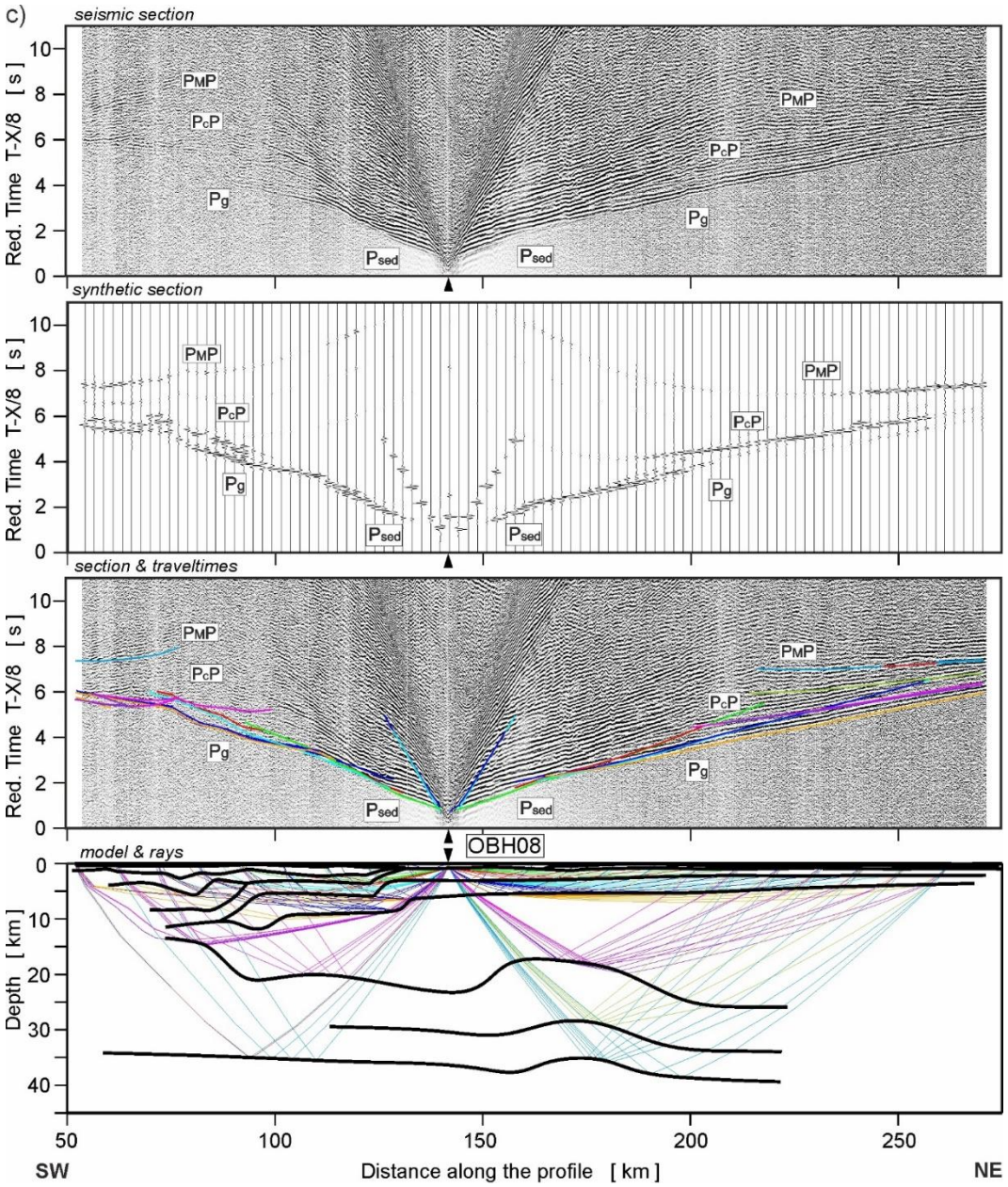

Fig. 5. (continued)

The discrepancies between the theoretical travel-times and the phase correlations on recorded marine seismic sections have reached as much as 0.5 s. For all the tested models, the upper boundary of the layer with velocities from 6.55 to 6.9 km/s is locally elevated to about 18 km depth for km 160-180 and km 60-80 of the profile. In the final Model 4 (Fig. 4), the depth of the Moho boundary gradually increases from ~35 km (km 58) to ~39 km (km 222) with a slight elevation (~3 km) repeating the geometry of the middle and lower crust boundaries.

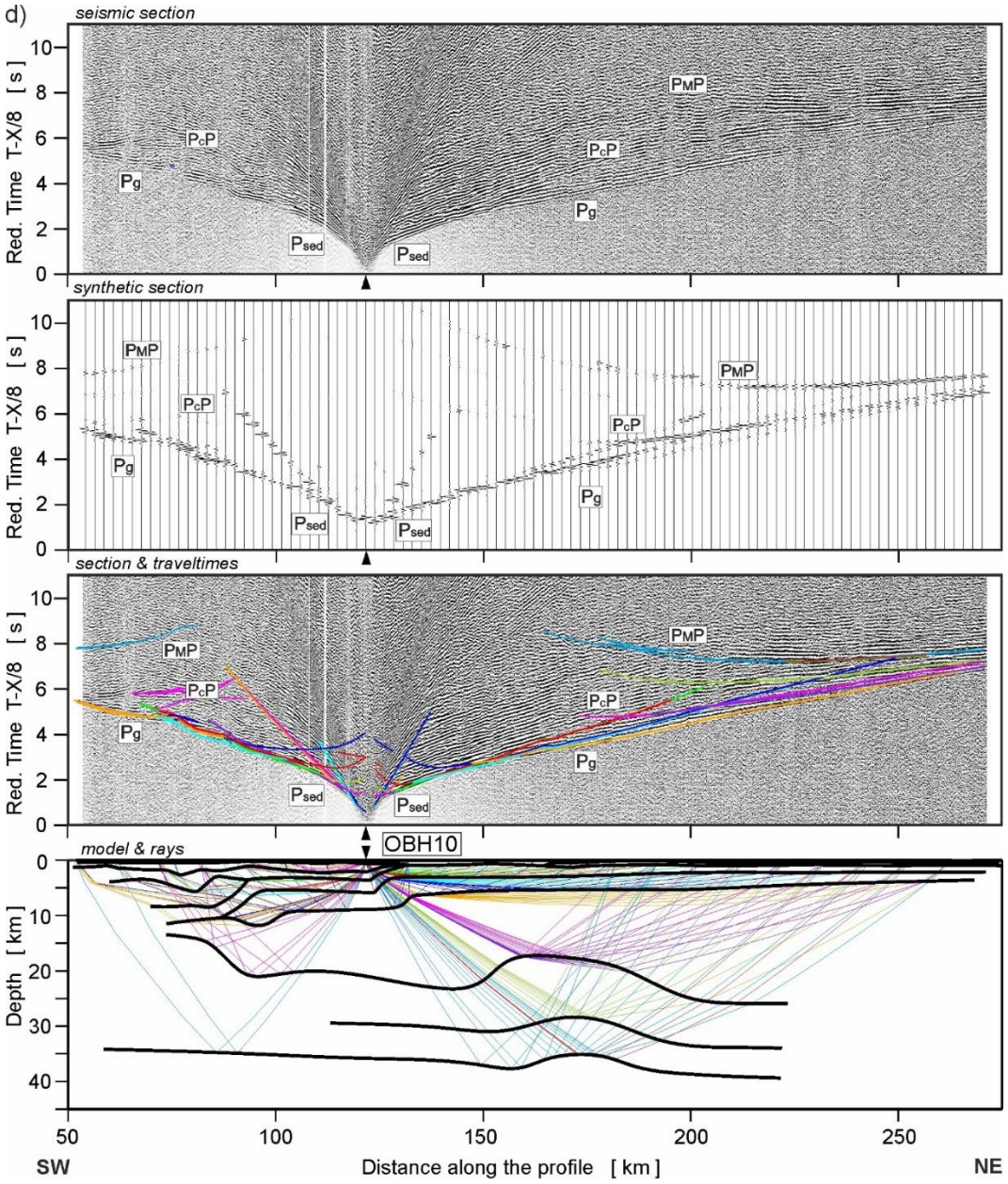

Fig. 5. (continued)

When assessing the quality of seismic modelling for these four models, Model 4 was rated the highest, with the best agreement of the theoretical and observed travel-times. The RMS residuals calculated for the P_MP phase as well as total RMS residuals for all discussed models are presented in Table 2. The synthetic seismograms calculated for the final model (Fig.5a-g) are generally in qualitative agreement with the observed seismograms. However, some differences are evident. In some of the presented examples, the P_g to P_cP relationship is not reproduced very well for certain offset intervals, especially between 80 and 140 km of the profile.

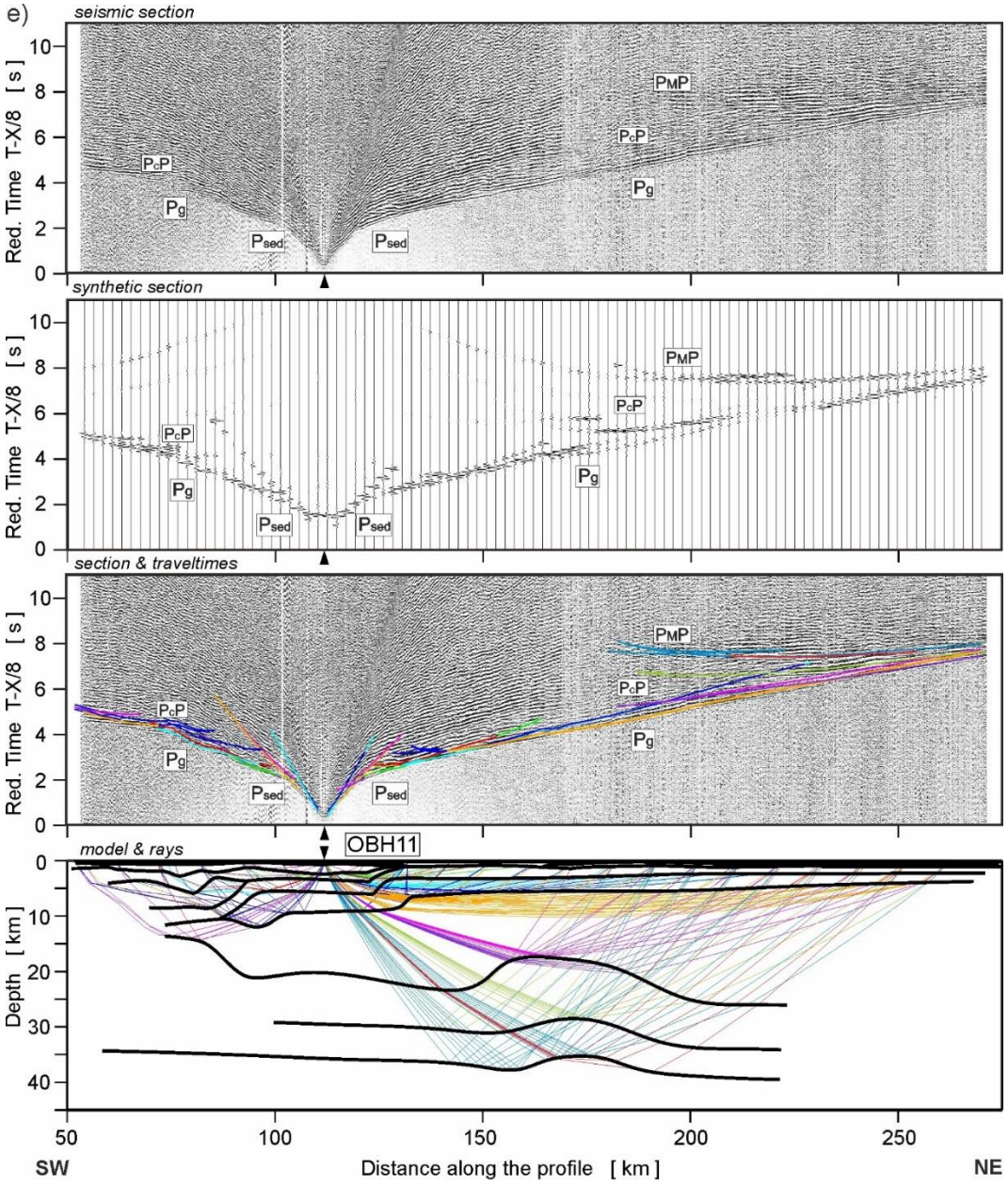

Fig. 5. (continued)

We ascribe the discrepancies mainly to be caused by imperfections in the model, but also to the use of ray-tracing techniques for the calculation of synthetic seismograms for a complex model. The synthetic seismograms show relatively small amplitudes for the upper mantle refraction. This may explain why the expected short branches of the P_n refraction arrivals are invisible against the background noise.

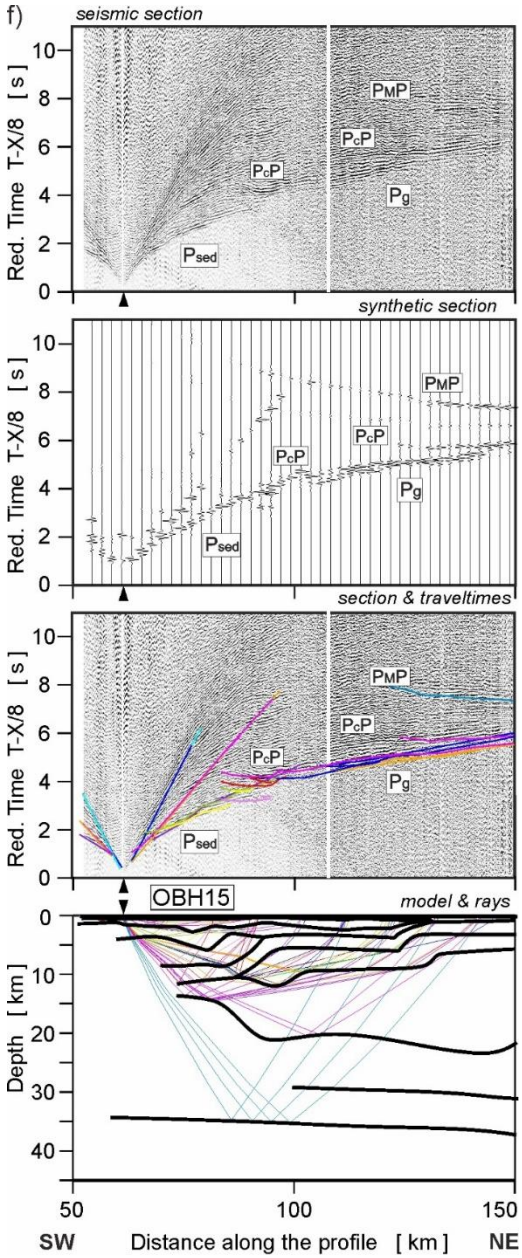

Fig. 5. (continued)

5.2. Uncertainty of the trial-and-error model

The uncertainty analysis of the seismic model is crucial from the point of view of its reliability. Several factors, including the quality of seismic data, signal-to-noise ratio as well as shots-and-receivers spacing influence the resolution and uncertainty of the model. The amount of seismic energy generated during shots has also an important role, especially for determining seismic velocities of the deeper-lying structures. We can assess the accuracy of the forward trail-and-error model in many ways, by, for example, considering the difference between the travel-time arrivals picked on the seismic sections against those calculated based on the model, or by examining the seismic ray density.

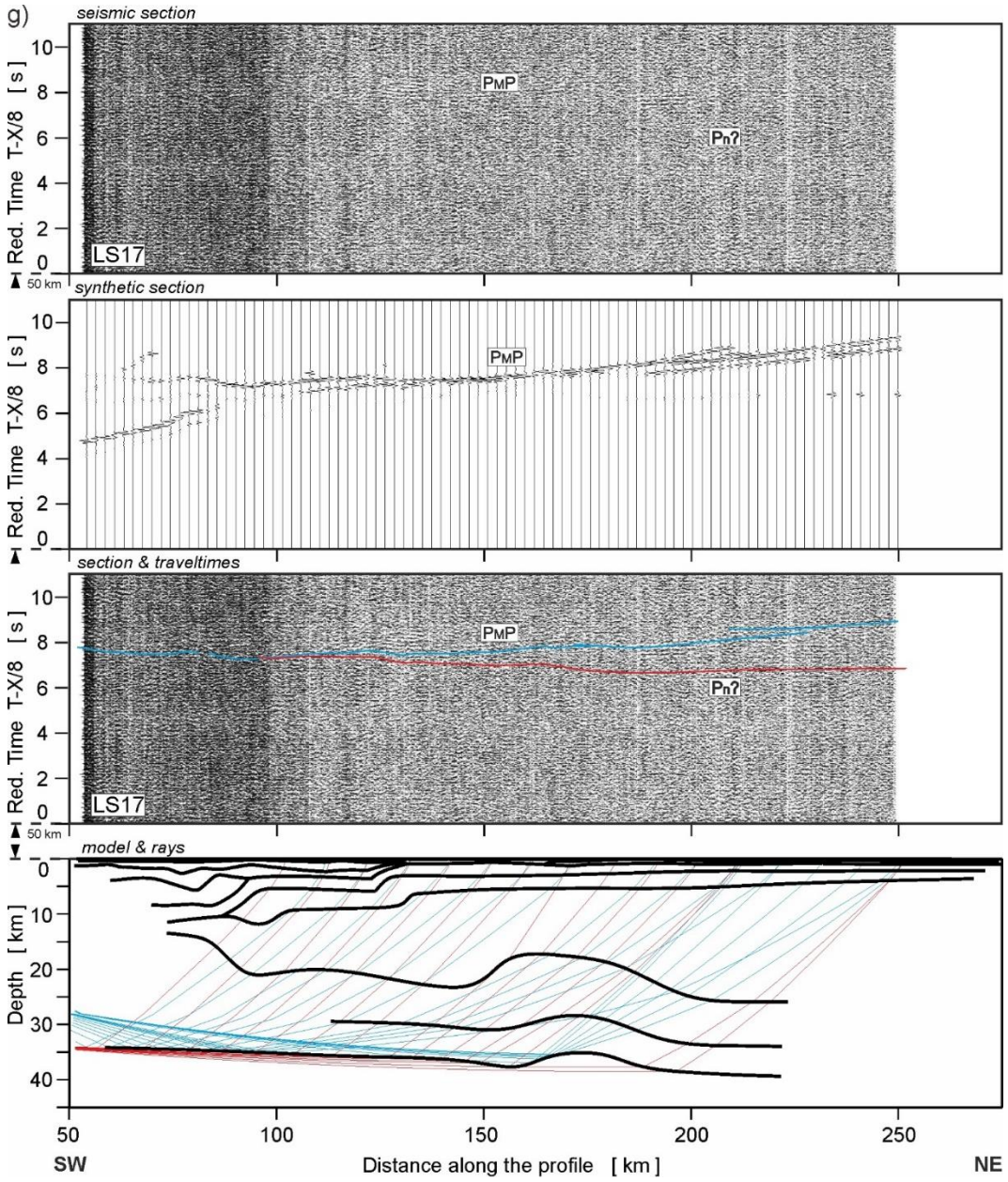

Fig. 5. (continued)

The density of the receiver points is a factor that determines the model degree of freedom. A higher density of receiver points imposes tighter constraints on a model that fits the data from different shot-gathers equally well. Considering the quality of this dataset, estimated uncertainty of travel-time picks varies between 50 and 150 ms with an average of 64 ms. These uncertainties are increasing with offset and decrease of signal to noise ratio. They are also larger for reflected phases. More detailed estimates are included in Table 3.

Table 2. RMS residuals calculated for the tested models. Besides total values for all stations, RMS values are presented separately for P_MP phase.

MODEL NUMBER	P_MP RMS [s] FOR STATION LS17	TOTAL P_MP RMS [s]	NUMBER OF P_MP PICKS	TOTAL RMS [s]	TOTAL NUMBER OF PICKS
Model 1	1.00	0.31	268	0.11	8227
Model 2	0.12	0.26	762	0.11	7869
Model 3	0.31	0.3	976	0.12	10035
Model 4 (preferred)	0.15	0.16	745	0.07	10532

The uncertainty analysis of the forward-ray-tracing model is presented in Figure 6. The detailed phase by phase uncertainty values for the final Model 4 are presented in Table 3. It should be noted that the sedimentary cover (6711 picked travel-time arrivals) has a much better ray coverage when compared to the underlying crystalline crustal layers. The uncertainty values for refraction in the crust (P_g phase) are presented in Table 3 separately for upper, middle, and lower crust. The upper crust has the highest number of 2654 travel-time arrivals picked. The RMS error for all refracted phases is below or equal 0.1 s.

Table 3. Number of picks and uncertainty values for all phases used in the trial-and-error forward modelling.

PHASE	NUMBER OF PICKS	ESTIMATED PICKING UNCERTAINITY [s]	RMS [s]
P_{sed} – C+M+UP+LP1+LP2	6711	0.05	0.06
P_g - upper crust	2654	0.07	0.06
P_g - middle crust	201	0.09	0.07
P_g – lower crust	74	0.09	0.1
P_cP – top of middle crust	70	0.12	0.17
P_cP – top of lower crust	77	0.12	0.11
P_MP	745	0.15	0.16
TOTAL	10532	0.064	0.07

The intracrustal reflections are observed only for the middle and lower crust. Given a low amplitude of intracrustal reflections, we were able to confidently determine only 147 travel-time arrivals. The clearest reflected phase with the highest amplitude is the Moho reflection (P_MP). This seismic phase is visible on most shot-gathers which allows for a reliable depth imaging of the Moho boundary along the entire length of the profile. The fitting accuracy of the observed versus calculated P_MP reflections is slightly lower than for refracted phases as its signal is much wider and therefore more difficult to pick. The RMS error is 0.16 s for 745 P_MP travel-time arrivals. The average RMS error for refracted and reflected phases is reasonably low and equals 0.07 s for a total of 10532 travel-time picked arrivals.

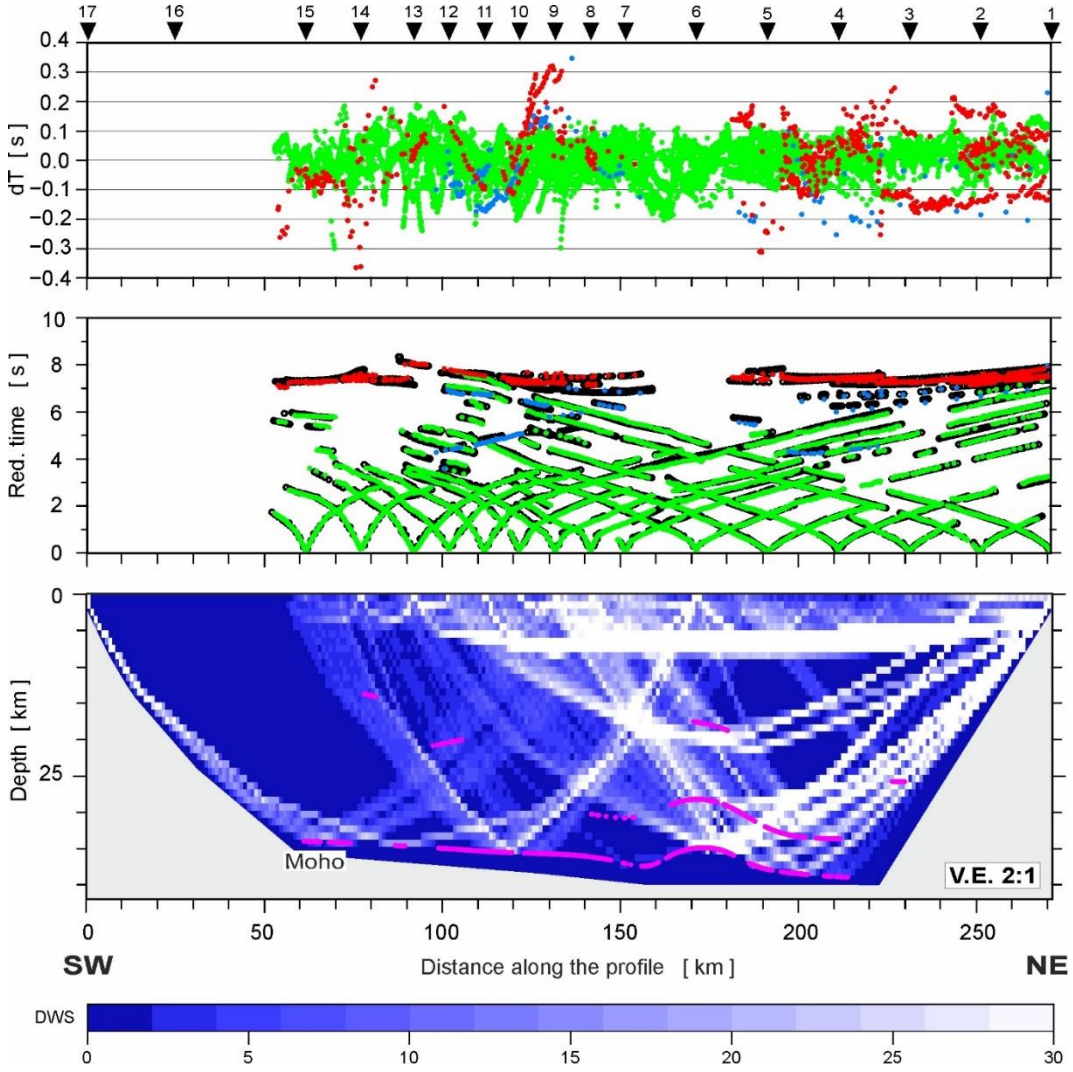

Fig. 6. Diagrams showing: (top) travel-time residuals, (middle) theoretical and observed travel-times and (bottom) ray coverage from forward modelling along the profile. Green points – P_g arrivals, blue points - P_cP arrivals, red points - P_MP arrivals, black circles – theoretical travel-times. The magenta points plotted along the interfaces mark the bottoming points of the modelled reflected phases (every third point is plotted) and their density is a measure of the location accuracy of the reflectors. DWS – derivative weight sum. Reduction velocity is 8 km/s.

6. Potential field modelling

Modelling for this study was carried out using the Geosoft GMSYS 2-D forward modelling package (Seequent, 2021) with model layers of infinite length. The modelling technique enabled the conversion of seismically interpreted horizons into geological bodies within the model. Each of these bodies appeared as a polygon with a density and magnetic susceptibility assigned. The software forward calculated the gravity and magnetic response of the model, using the techniques outlined in Talwani and Ewing (1960). The gravity and magnetic responses of the proposed model were calculated and compared with the observed gravity and magnetic profiles (Fig. 7); then the model was interactively adjusted until

a fit between the synthetic response and the observed gravity and magnetic profiles was obtained. We used the free-air gravity anomalies for modelling the offshore part of the profile and Bouguer gravity anomalies for the minor onshore section between stations LS16 and LS17 (Fig. 2b). The use of a seismic P-wave velocity model to constrain the geometry and density of model bodies minimized the number of possible solutions. Seismic velocities were recalculated to densities using the Nafe-Drake formula (Ludwig et al., 1970; Brocher, 2005). The starting susceptibility values for the magnetic basement were adopted from previous modelling studies (Petecki, 2002, Mazur et al., 2016).

In our first gravity and magnetic model, we accepted relatively large mean errors of nearly 15 mGal and 110 nT (Fig. 7) to preserve original geometries of both major velocity discontinuities and velocity isolines that defined the boundaries of the model bodies. We also retained densities as calculated directly from seismic velocities. The only minor departures from the seismic velocities were accepted for the SW section of the profile, which was not sufficiently covered by seismic rays (Fig. 5).

Three major areas of misfit were identified in the synthetic gravity model, numbered 1-3 in Figure 7. Misfit (1) is located in the Kołobrzeg Anticline (Dadlez, 1993), a tectonic structure created by the Late Cretaceous – early Paleogene inversion of the MPT (Dadlez et al., 1997). Also, other deep seismic soundings carried out onshore Poland (see Guterch and Grad, 2006, for the overview) poorly imaged shallow inversion structures developed in the Permian-Mesozoic strata of the Polish Basin. Misfit (2) corresponds to the area, where a synthetic response of the model was unable to replicate a long-wavelength gravity low in the vicinity of the TTZ. Similar gravity lows, associated with the TTZ, were reported from central and northern Poland (Mazur et al., 2015, 2016). Finally, misfit (3) indicates a laterally extensive mass deficit along the entire NE section of the gravity model. However, misfit (3) may be also induced by the presence of misfit (2).

The synthetic magnetic profile is smooth owing to a simple susceptibility structure assumed (Fig. 7). Despite that, the susceptibilities in the seismically defined model bodies were adjusted to reduce the misfit between the synthetic profile and observed data. Due to the lack of intra-sedimentary volcanics, the magnetic response along the profile must be mostly controlled by a depth to crystalline basement. Indeed, the profile indicates that the seismic modelling correctly revealed the position of the magnetic (crystalline) basement. Also, the location and geometry of a top basement slope beneath the Caledonian Deformation Front (cf. Mazur et al., 2016), indicated by the seismic velocity model, is confirmed by an acceptable match between the model response and observed magnetic profile (Fig. 7).

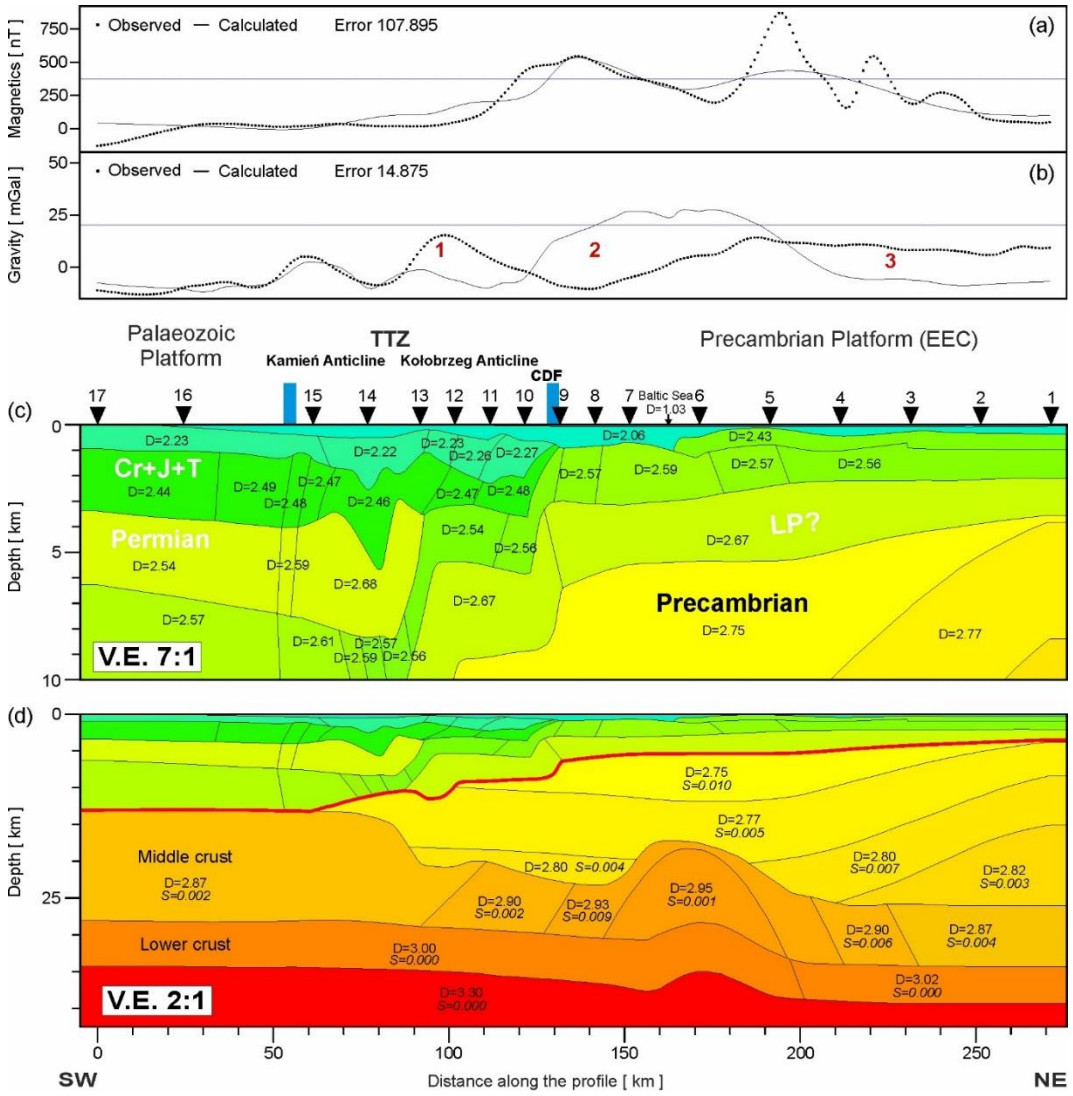

Fig. 7. Two-dimensional gravity and magnetic model for the BalTec profile. (a, b) Magnetic and gravity data, respectively. Dotted lines – observed and thin solid lines – modelled. (c) – vertically exaggerated (7:1) upper part of the geological model. (d) – vertically exaggerated (2:1) full geological model based on the seismic refraction profile. Thick red line in (d) represents the top of crystalline basement. Numbers indicate densities (D) in g/cm^3 and susceptibilities (S) in cgs convention (italic). Densities are calculated from seismic velocities using the Nafe-Drake formula. CDF – Caledonian Deformation Front. 1, 2, 3 – location of main misfits between the observed gravity profile and synthetic response of the model.

The model was unable to replicate short-wavelength, high-amplitude magnetic anomalies in the ENE section of the profile. They probably represent iron oxides mineralisation in the crystalline basement of the EEC (Kubicki, 1984) or a pattern of magnetic anomalies associated with the early Mesoproterozoic AMCG magmatism (Petecki and Rosowiecka, 2017). The lack of geological data precludes a definite interpretation. Therefore, adjusting the synthetic magnetic profile to the observed short wavelength anomalies would require splitting the geological model, without a sufficient justification, into narrow, vertical blocks with contrasting susceptibility.

As a next step, an attempt was made to reduce some of the observed misfits and evaluate the quality of the seismic velocity model. A key problem revealed by the gravity data is apparently associated with misfit (2) that comes about along the section of the profile between km 120 and 200. To tackle this problem, we produced two models that reduce the misfit between the observed and forward modelled gravity profiles (Fig. 8). We have not favoured any of them since the potential field modelling is non-unique and different crustal architectures may produce a similar fit between the observed and synthetic data. Both density models match the main characteristics of the observed gravity field and reduce an error below an acceptable level of 5 mGal. The models are both geologically viable and refer to the concepts previously presented in the regional literature.

While building our interpretative gravity and magnetic models, we did not alter the geometry of interfaces inherited from the original velocity model, apart from minor adjustments in the under-constrained SW section of the profile. However, using a trial-and-error approach, we introduced additional model bodies based on the modified density model. The densities of new bodies are geologically realistic but depart from those that were directly calculated out of seismic velocities by means of the Nafe-Drake formula. Model (Fig. 8a) explains the high-velocity zone in the middle crust as an anorthosite body that can have velocities around 6.8 km/s but, at the same time, has comparatively low density values. The intrusion inferred resides in the middle crust between km 120 and 200 of the profile i.e., in the section that originally produced misfit (2). Similarly, a major mafic intrusion was interpreted by Thybo (2001) within the Sorgenfrei-Tornquist Zone at the transition from the WEP to the Baltic Shield proper. In model (Fig 8b), a crustal keel replaces the intrusion between km 135 and 190 of the profile. A comparable crustal keel was previously postulated within the Sorgenfrei-Tornquist and Teisseyre-Tornquist Zones (BABEL Working Group, 1991, 1993; Makris and Wang, 1994; Thybo, 2000; Mazur et al., 2016). In this study, the keel is interpreted to represent magmatic underplating as in Thybo (2000) rather than a fossil lower crustal suture (Mazur et al., 2016).

7. Discussion

The major objective addressed by the BalTec profile was the determination of the P-wave velocity distribution in the lower crust beneath the Baltic Sea south of Bornholm. Due to the limited length of this profile and the absence of waves from the middle and lower crust on seismic sections, this could not have been achieved along the entire profile. The modelling of the Moho boundary (Fig. 4) was possible owing to well resolved P_MP waves in most record sections (Figs. 5a-f).

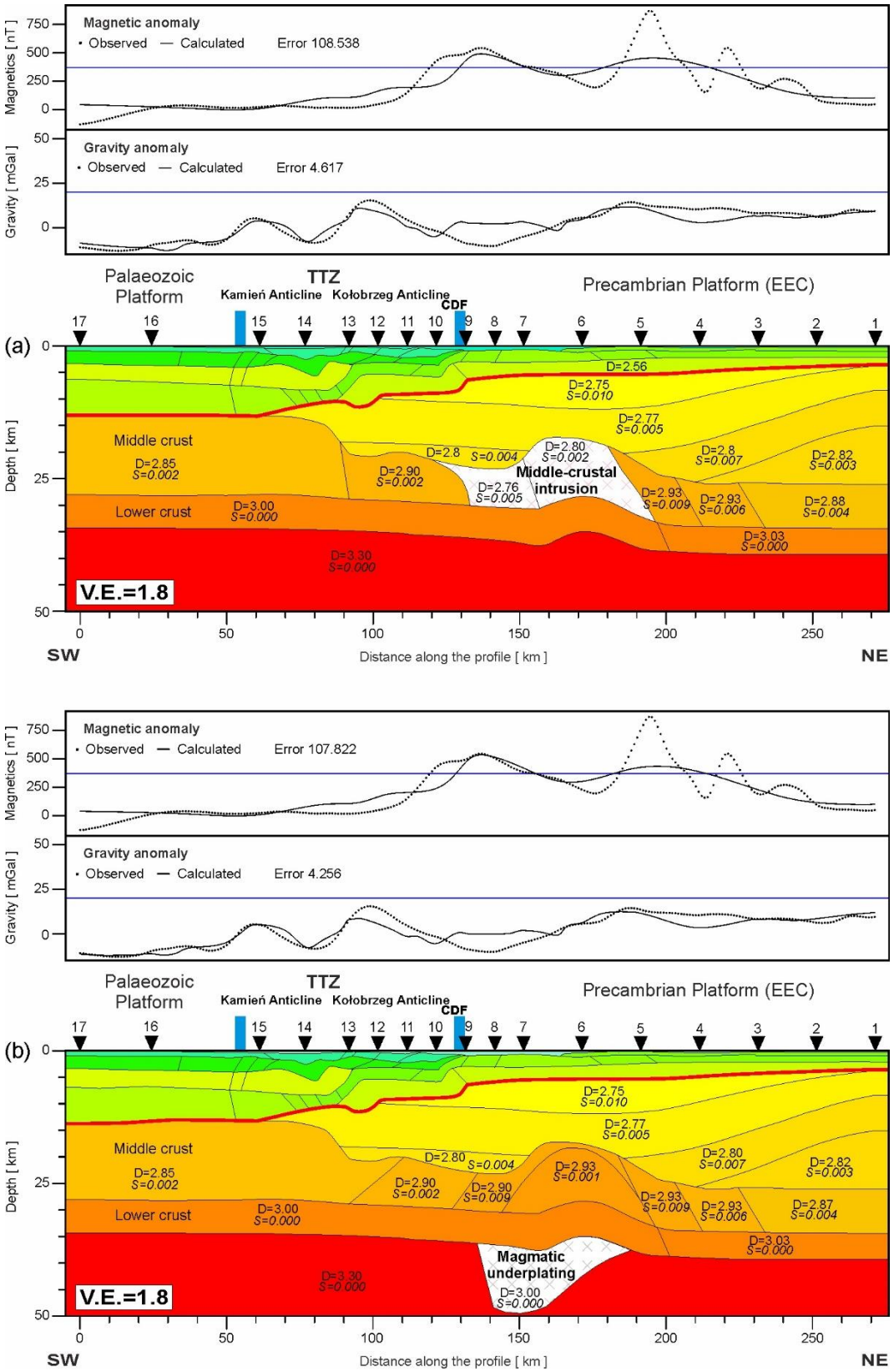

Fig. 8. Two models that reduce the misfit between the observed and forward modelled gravity profiles. Both density models match the main characteristics of the observed gravity field and reduce an error below an acceptable level of 5 mGal. Additio nal model bodies are introduced compared to the initial gravity and magnetic model of Figure 7. The densities of the new bodies

depart from those that were directly calculated out of seismic velocities by means of the Nafe-Drake formula. Model (a) explains the high-velocity zone in the middle crust as an intrusive anorthosite body with velocities around 6.8 km/s and, at the same time, comparatively low densities. The intrusion inferred resides in the middle crust between km 120 and 200 of the profile, i.e., in the section corresponding to misfit (2) in Figure 7. In model (8b), a crustal keel replaces the intrusion between km 135 and 190 of the profile. The keel is intended to represent magmatic underplating (Thybo, 2000) rather than a fossil lower crustal suture (Mazur et al., 2016). Dotted lines – observed and thin solid lines – modelled data in gravity and magnetic panels. Thick red line represents the top of the crystalline basement. Numbers indicate densities in g/cm^3 and susceptibilities in cgs convention (italic). CDF – Caledonian Deformation Front.

In the previously performed experiments in this part of the South Baltic Sea, TTZ'92 (Makris and Wang, 1994) and BASIN'96 (Bleibinhaus et al., 1999) (Fig. 1), V_p for the lower crust is higher or lower than 7 km/s, respectively. In the light of our experience with seismic modelling of the BalTec profile, it seems that modelling at depths exceeding ~10 km must be based on assumptions about velocity in deeper structures. The same must have been the case with the TTZ'92/II (Makris and Wang, 1994) and PQ2-001/002 (Bleibinhaus et al., 1999) marine profiles closest to BalTec, which are even shorter than the BalTec profile. In the model presented by Makris and Wang (1994), there are high velocities at the bottom of the crust (V_p >7 km/s), although the gradient used, resulting in a velocity of 7.5 km/s above the Moho, seems excessively high. The model proposed by Bleibinhaus et al. (1999), based on limited data, postulates V_p = 6.7 km/s and <6.7 km/s for the lower crust at the extremities and centre of the section, respectively. After tests, we found the parameters used by Bleibinhaus et al. (1999) and Makris and Wang (1994) not applicable to our model. In addition, BABEL line A, whose SW extremity crosses the STZ, reveals a lower crustal velocity in that area, in the range of 7.0-7.2 km/s (Abramovitz et al., 1997). FENNOLORA models (Luosto, 1997) show V_p = 7.1-7.25 km/s in the lower crust for the craton, and V_p ~6.6 km/s for the Caledonian basement in northern Germany (Guggisberg et al., 1991). The latter includes a low P-wave velocity zone (V_p = 6.4-6.6 km/s) in the lower crust along the Caledonian suture that cannot be easily attributed to Avalonia or Baltica (Bayer et al., 2002; Smit et al., 2016). The low velocity zone was interpreted by Smit et al. (2016) as a hitherto unrecognized crustal segment (accretionary complex) that separates Avalonia from Baltica. Nevertheless, the BalTec profile does not reach this zone, being located farther NE. In the western part of Fennoscandia, all profiles acquired on the EEC and crossing the Teisseyre-Tornquist Zone have a tripartite crystalline crust with V_p velocities for the lower crust in the range of 7.0 ± 0.2 km/s. There is no reason to assume that the BalTec profile is different, both in the cratonic and TTZ parts of the model. Additionally, this is confirmed by the information from models calculated for the nearest perpendicular land profiles, TTZ (Grad et al., 1999 and Janik et al., 2005) and P3 (Środa et al., 1999). In the TTZ profile, a similar type of crust but with smaller thicknesses is observed.

If a misfit of the gravity model related to the Kołobrzeg Anticline seems obvious, the remaining two areas of mismatch (Fig. 7) require some additional discussion. The problem of a gravity low associated with the Teisseyre-Tornquist Zone onshore of central and northern Poland was solved in recent modelling studies by introducing a crustal keel (Mazur et al., 2015, 2016), i.e., a relatively short-wavelength Moho depression. The concept of the keel itself was first proposed by interpreters of the BABEL A seismic profile (BABEL Working Group, 1991, 1993) and then elucidated by Thybo et al. (1994) and Thybo (2000). A crustal keel was also shown as an alternative interpretation of the P4 seismic profile (Grad et al., 2003). The authors advocating the presence of the keel suggested various geological interpretations of its origin (see Mazur et al., 2016 for an overview). However, some seismic studies including ours did not reveal the existence of the keel, e.g., LT-7 (Guterch et al., 1994), DEKORP-PQ (Krawczyk et al., 2002) and BalTec profile (Fig. 4). Nevertheless, the model shown in Figure 8b demonstrates that the implementation of a crustal keel or magmatic underplating allows to significantly reduce the misfit in a gravity model also in the case of the BalTec profile. Alternatively, the misfit can be related to the occurrence of a low-density body in the middle crust as, for instance, a large igneous intrusion (Fig. 8a). Nevertheless, a magnetic anomaly potentially manifesting the presence of magmatic rocks is largely lacking unless the intrusion might be partly below the Curie isotherm. Whatever the reason for the misfit is, the relatively good match of the magnetic response of the model precludes its relationship to any important inaccuracy in the position of the crystalline basement. Finally, Figure 8 shows that fixing misfit (2) also eliminates misfit (3) that appears to be a secondary effect of mass excess in the TTZ.

In terms of geological interpretation, the BalTec model shows a continuity of the lower and middle crust along most of the profile besides the seismically unconstrained SW section (Figs. 7, 9). On the contrary, important perturbations are observed within the upper crust and the overlying sedimentary cover. The cratonic upper crust shows an overall thinning from the NE to km 60 of the profile, where it disappears (Figs. 7, 9). Farther SW, between km 0 and 60, an up to 13-km-thick series of Phanerozoic sedimentary rocks is inferred by comparison with the neighbouring WARR land profiles (Guterch et al., 1994; Grad et al., 1999). Consequently, Phanerozoic sediments are much thicker between km 0 and 60 than along the remainder of the profile. The obvious explanation of this phenomenon is the Permian-Mesozoic continental rifting and extension as 50-150 km section of the model corresponds to the offshore continuation of the MPT. However, the total thickness of Permian and younger sediments at the WSW extremity of the model is in the range of 6-7 km, i.e., represents only 50 % of the subsidence observed. The remaining sediments must be pre-Permian in age and may represent a cumulative effect of two geological events. The younger was crustal stretching at the passive Laurussia margin during the Devonian and Carboniferous (see Smit et al., 2018 for a recent overview). This event is probably superimposed on earlier Silurian subsidence in front of the advancing Caledonian orogen. Based on

evidence from the nearby Rügen Island (e.g., Dallmeyer et al., 1999), an important share of pre-Permian sediments may represent tectonically duplicated Ordovician sediments of the Caledonian orogenic wedge. An important feature illustrated by the BalTec profile is a slope of crystalline basement coinciding with the CDF (Figs. 7-9). This confirms the results of earlier geophysical study by Mazur et al. (2016) and suggests a buttressing effect of the EEC basement on the eastward extent of the early Palaeozoic deformation.

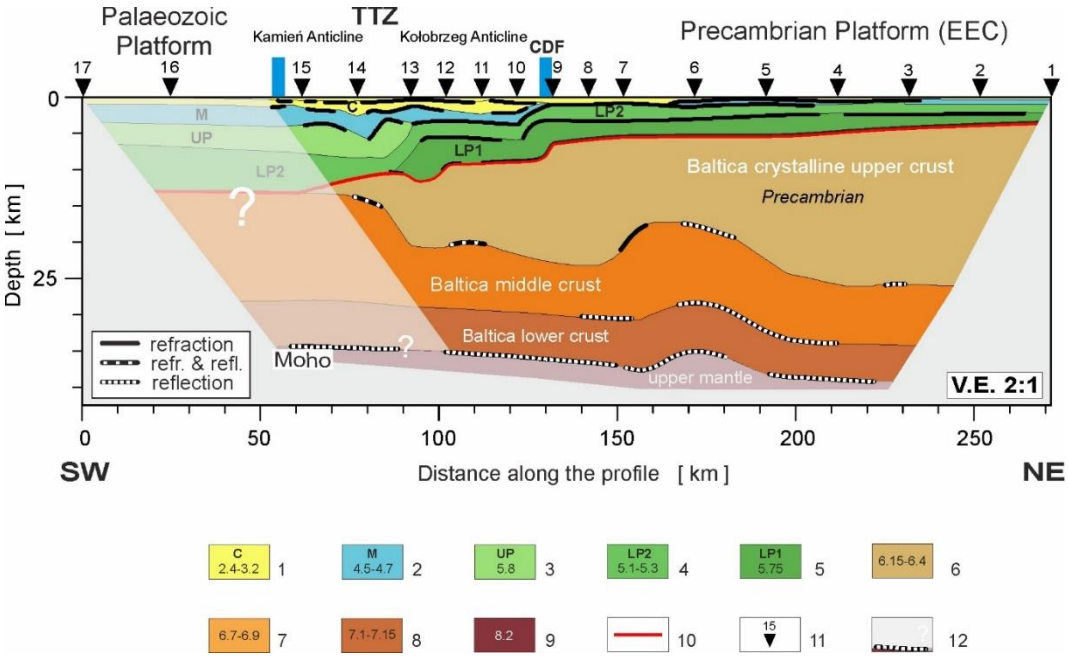

Fig. 9. Simplified sketch of the crustal structure derived along the BalTec profile. (1) C - Cenozoic post-inversion sediments, (2.4-3.2 km/s); (2) M - Mesozoic sediments of the Southern Permian Basin, (4.5-4.7 km/s); (3) UP - Upper Palaeozoic sediments of the Laurussia passive margin, (5.8 km/s); (4) LP2 - Lower Palaeozoic sediments of the Caledonian Foreland Basin (NE part) and Caledonian orogenic wedge (SW part) undivided, (5.1-5.3 km/s); (5) LP1 - Lower Palaeozoic sediments of the Baltica passive margin and Caledonian Foreland Basin, (5.7 km/s); (6) Baltica crystalline upper crust (6.15-6.4 km/s); (7) Baltica middle crust, (6.7-6.9 km/s); (8) Baltica lower crust (7.1-7.15 km/s); (9) uppermost mantle (8.2 km/s); (10) Top of the Precambrian basement; (11) location of the OBH and land stations; (12) A semi-transparent polygon represents the part of the model that is not sufficiently covered by seismic rays. The numbers in the colour boxes are P-wave velocity values in km/s. Thick blue lines show the range of the TTZ.

The section with no upper Baltica crust between km 0 and 60 of the profile corresponds to a zone of low ray coverage (grey zone in Fig. 9). Therefore, the lack of the cratonic upper crust in this area remains uncertain. Nevertheless, such a model, if confirmed, would be geologically feasible since the MPT, crossed by the profile, does not reveal all features typical of the other Permian-Mesozoic depocenters in NW Europe and continental rifts in general (e.g., Zeyen et al., 1997; Scheck-Wenderoth and Lamarche, 2005; Maystrenko and Scheck-Wenderoth, 2013). There was no volcanism associated with the

formation of the MPT and the Moho was not elevated underneath the MPT (Figs. 7, 9). Recent numerical modelling studies show important control of the integrated brittle strength of the lithosphere on a rifting style (Naliboff and Buiter, 2015; Yang et al., 2018). In the case of the MPT with a relatively thin crust (Fig. 4), the integrated brittle strength must have been controlled by the lithospheric mantle. Indeed, the Polish Basin is characterized by NE-ward thickening of the lithospheric mantle toward the interior of the EEC (Mazur et al., 2021). Therefore, the lithospheric mantle directly beneath the MPT was probably too strong to extend but, instead, the thinner lithosphere farther west was weak enough to be stretched. By analogy to the model by Yang et al. (2018), Mazur et al. (2021) suggested that the extension was offset from the shallow MPT in the east to the lower crust and sub-Moho lithosphere in W Poland and NE Germany. In accord with Naliboff and Buiter (2015) and Yang et al. (2018), they concluded that the location of the pre-existing weakness zone (TTZ) relative to a change in lithosphere thickness may localise a rift graben (MPT) within the upper crust and shift the magmatism and deeper lithospheric extension away from the upper crustal expression of the rift.

Whether or not the upper crust was eliminated, our results suggest a continuation of the Baltica middle and lower crust through the TTZ in the southern Baltic Sea (Fig. 9) in agreement with the previous seismic (Lassen et al., 2001; Krawczyk et al., 2002; Bayer et al., 2002) and potential field studies (Thybo, 2001; Banka et al., 2002; Dehghan et al., 2021). Consequently, the TTZ is not a crustal scale tectonic suture and does not coincide with the edge of the EEC in the southern Baltic Sea. Furthermore, the CDF must be of thin-skinned character involving only lower Palaeozoic sediments overlying the Precambrian basement (c.f., Mazur et al., 2016). Therefore, the Thor Suture between Baltica and East Avalonia at the middle and lower crustal level seems to be located farther SW, beyond the ending of the BalTec profile (c.f., Bayer et al., 2002). Instead, the profile seems to crosscut the Caledonian suture within the lower Palaeozoic sediments somewhere between the Ordovician deposits of Rügen, having an Avalonia affinity (e.g., Katzung et al., 1995; Dallmeyer et al., 1999), and the CDF (Figs 1, 2). However, the precise location of the suture within the Palaeozoic sediments has not been recognised due to the resolution of the WARR data. Therefore, it remains uncertain to what extent the BalTec profile crosscuts the Ordovician sediments, forming a Caledonian accretionary wedge in the vicinity of Rügen (e.g., Dallmeyer et al., 1999). In our interpretation (Fig. 9) these sediments, if present at the WSW extremity of the profile, are merged with the Ordovician and Silurian deposits of a Caledonian foreland basin, showing a clear affinity to Baltica in the boreholes located onshore Poland (Poprawa, 2006).

Our interpretation is generally consistent with seismological data collected in the course of the PASSEQ passive experiment (2006-2008; see Wilde-Piórko et al., 2008). These data showed no general and abrupt change in the splitting parameters (anisotropic structure) related to the TTZ, marking the limit of the Precambrian Platform at the surface (Vecsey et al., 2014). The coherence of anisotropic signals

supports a SW-ward continuation of the Precambrian mantle lithosphere beneath the TESZ and the adjacent Phanerozoic part of Europe, probably as far as towards the Bohemian Massif (Vecsey et al., 2014).

The geometry of the velocity model suggests the presence of two zones of perturbations within the upper crust and the overlying sedimentary cover, intersected by the BalTec profile (Fig. 9). The position of the eastern one (km 120-135) coincides with the CDF and Koszalin Fault. The western discontinuity (km 75-90) corresponds to the flank of the Gryfice Graben that was reactivated by the Late Cretaceous inversion. The vergence of the western zone is consistent with its possible inversion-related origin (Dadlez, 1993; Seidel et al., 2018). The vergence of the eastern zone (Fig. 9) is more enigmatic since it seems to be opposite to that of the CDF and the Koszalin Fault as interpreted in the reflection seismic data (Jaworowski et al., 2010, Krzywiec et al., 2003; Mazur et al., 2016). Therefore, it might be rather related to the Devonian-Carboniferous, post-Caledonian uplift of the EEC margin (Botor et al., 2021).

8. Conclusions

Our study confirms earlier observations on the lack of a crustal-scale discontinuity associated with the TTZ (Lassen et al., 2001; Thybo, 2001; Krawczyk et al., 2002; Bayer et al., 2002; Dehghan et al., 2021). Despite insufficient seismic control on the SW section of the BalTec profile, our results suggest a SW-ward continuation of the Baltica middle and lower crust through the TTZ (Fig. 9). This seems to preclude the coincidence of the Caledonian Thor suture with the TTZ. Instead, the latter shows an important perturbation of the upper crust and sedimentary cover (Fig. 9). Nevertheless, this seems to be mostly associated with the superimposed effects of Devonian-Carboniferous and Permian-Mesozoic extension (Krzywiec et al., 2021) and post-Caledonian Carboniferous uplift of the EEC (Botor et al., 2021). The only conspicuous compressional event imaged by our data is the Late Cretaceous-Paleogene inversion of the Permian-Mesozoic basin (Krzywiec et al., 2021). Our WARR data provide no evidence for the Caledonian and Variscan shortening including the Caledonian Deformation Front.

The compilation of the seismic and potential field data indicates the presence of an anomalous feature associated with the NE boundary of the TTZ. This was already suggested by an apparent conflict between the seismic interpretations by Bleibinhaus et al. (1999) and Makris and Wang (1994). The former authors postulate the low seismic velocities (6.7 km/s) in that area down to the Moho that is smooth and relatively shallow. In contrast, the latter researchers interpret high P-wave velocities (up to 7.5 km/s) in the lower crust that are compensated by a crustal keel. Our study highlighted the same problem since the smooth Moho associated with a relatively high seismic velocity (7.12 km/s; Fig. 4) must unavoidably produce a mass excess in the gravity model (Fig. 7). We offer two alternative solutions (Fig. 8): (1) a middle crustal intrusive body (compare Thybo, 2001), or (2) a crustal keel (BABEL

Working Group, 1991, 1993; Makris and Wang, 1994; Thybo, 2000; Mazur et al., 2016) that have to be tested in the course of further studies.

Acknowledgements

This study was funded by the Polish National Science Centre grant no UMO-2017/27/B/ST10/02316. Participation of the Polish group at field work was supported by a subsidy from the Polish Ministry of Education and Science for the Institute of Geophysics, Polish Academy of Sciences. Cruise MSM52 has been funded by German Science Foundation DFG and Federal Ministry of Education and Research (BMBF). We thank Joachim Buelow, Volkmar Damm, Vera Noack and the Federal Institute for Geosciences and Natural Resources (BGR) and Jarosław Grzyb (IGF PAS) for their support during seismic data acquisition. The public domain GMT package (Wessel and Smith, 1995) was used to produce some of the figures. The authors wish to thank Frauke Klingelhoefer (Ifremer, Department of Marine Geosciences), Wolfram Geissler (Alfred Wegener Institute) and an Anonymous Reviewer for their constructive comments on an earlier version of this manuscript.

References

Abramovitz, T., Thybo, H., 2000. Seismic images of Caledonian, lithosphere-scale collision structures in the southeastern North Sea along Mona Lisa Profile 2. Tectonophysics 317 (1), 27–54.

Abramovitz, T., Berthelsen, A., Thybo, H., 1997. Proterozoic sutures and terranes in the southeastern Baltic Shield interpreted from BABEL deep seismic data. Tectonophysics 270, 259–277.

Abramovitz, T., Thybo, H., Mona Lisa Working Group, 1998. Seismic structure across the Caledonian Deformation Front along MONA LISA profile 1 in the southeastern North Sea. Tectonophysics 288 (1-4), 153–176.

Al Hseinat, M., Hübscher, C., 2017. Late Cretaceous to recent tectonic evolution of the North German Basin and the transition zone to the Baltic Shield/southwest Baltic Sea. Tectonophysics 708, 28–55.

BABEL Working Group, 1991. Deep seismic survey images the structure of the Tornquist Zone beneath the Southern Baltic Sea. Geophysical Research Letters 18, 1091–1094.

BABEL Working Group, 1993. Deep seismic reflection/refraction interpretation of crustal structure along BABEL profiles A and B in the southern Baltic Sea. Geophysical Journal International 112, 243–325.

Banka, D., Pharaoh, T.C., Williamson, J.P., TESZ Project Potential Field Core Group, 2002. Potential field imaging of Palaeozoic orogenic structure in northern and central Europe. Tectonophysics 360(1-4), 23–45.

Bayer, U., Grad, M., Pharaoh, T.C., Thybo, H., Guterch, A., Banka, D., Lamarche, J., Lassen, A., Lewerenz, B., Scheck, M. Marotta, A.M., 2002. The southern margin of the East European Craton: new results from seismic sounding and potential fields between the North Sea and Poland. Tectonophysics 360(1-4), 301–314.

Berthelsen, A., 1992. Mobile Europe. In: Blundell, D. J., Freeman, R., Mueller, S. (Eds.), A continent revealed: The European Geotraverse, Structure and Dynamic Evolution, pp. 11–32.

Berthelsen, A., 1998. The Tornquist Zone northwest of Carpathians: an intraplate pseudosuture. GFF 120, 223–230.

Bleibinhaus, F., Beilecke, T., Bram, K., Gebrande, H., 1999. A seismic velocity model for the SW Baltic Sea derived from BASIN'96 refraction seismic data. Tectonophysics 314, 269–283.

Bogdanova, S.V., Pashkevich, I.K., Gorbatschev, R., Orlyuk, M.I., 1996. Riphean rifting and major Palaeoproterozoic crustal boundaries in the basement of the East-European Craton: geology and geophysics. Tectonophysics 268, 1–21.

Botor, D., Mazur, S., Anczkiewicz, A.A., Dunkl, I., Golonka, J., 2021. Thermal history of the East European Platform margin in Poland based on apatite and zircon low-temperature thermochronology. Solid Earth 12 (8), 1899–1930.

Breitkreuz, C. Kennedy, A., Geißler, M., Ehling, B.-C., Kopp, J., Muszynski, A., Protas, A., Stouge, S., 2007. Far Eastern Avalonia: Its chronostratigraphic structure revealed by SHRIMP zircon ages from Upper Carboniferous to Lower Permian volcanic rocks (drill cores from Germany, Poland, and Denmark). In: Linnemann, U., Nance, R.D., Kraft, P., Zulauf, G. (Eds.), The evolution of the Rheic Ocean: From Avalonian-Cadomian active margin to Alleghenian-Variscan collision. Geological Society of America Special Paper 423, p. 173–190.

Brocher, T.M., 2005. Empirical relations between elastic wave speeds and density in the Earth's crust. Bulletin of the Seismological Society of America 95, 2081–2092.

Červený, P., and Pšenčík, I., 1983. SEIS83 - seismic program package.

Červený, V., Pšenčík, I., 1984. SEIS83 - Numerical modelling of seismic wave fields in 2-D laterally varying layered structures by the ray method, in: Engdal, E.R. (Ed.), Documentation of Earthquake Algorithms, Rep. SE-35, World Data Cent. A for Solid Earth Geophysics, Boulder, Colo., 36–40.

Cocks, L. R. M., Fortey, R. A., 1998. The Lower Palaeozoic margins of Baltica. GFF 120, 173–179.

Dadlez, R., 1993. Pre-Cainozoic tectonics of the southern Baltic Sea. Geological Quarterly, 37(3), 431–450.

Dadlez, R., Jóźwiak, W., Młynarski, S., 1997. Subsidence and inversion in the western part of Polish Basin-data from seismic velocities. Geological Quarterly 41 (2), 197–208.

Dadlez, R., Grad, M., Guterch, A., 2005. Crustal structure below the Polish Basin: is it composed of proximal terranes derived from Baltica? Tectonophysics 411 (1–4), 111–128.

Dehghan, M.J., Ardestani, V.E., Dehghani, A., 2021. The study of crustal structures in the southwestern part of the Baltic Sea by modeling of gravity data. Arabian Journal of Geosciences 14(5), 1–16.

Dallmeyer, R.D., Giese, U., Glasmacher, U., Pickel, W., 1999. First $^{40}Ar/^{39}Ar$ age constraints for the Caledonian evolution of the Trans-European suture zone in NE Germany. Journal of the Geological Society 156 (2), 279–290.

DEKORP-BASIN Research Group, 1998. Survey provides seismic insights into an old suture zone. EOS 79, 151–159.

DEKORP-BASIN Research Group, 1999. Deep crustal structure of the Northeast German basin: New DEKORP-BASIN '96 deep profiling results. Geology 27, 55–58.

Erlström, M., Thomas, S.A., Deeks, N., Sivhed, U., 1997. Structure and tectonic evolution of the Tornquist Zone and adjacent sedimentary basins in Scania and the southern Baltic Sea area. Tectonophysics 271 (3-4), 191–215.

EUGENO-S Working Group, 1988. Crustal structure and tectonic evaluation of the transition between the Baltic Shield and the North German Caledonides (The EUGENO-S Project). Tectonophysics 150, 253–348.

Franke, D., 1994. The deformational history of the Caledonian terranes at Baltica's southwest margin. Zeitschrift fur Geologische Wissenschaften 22, 67–80.

Gossler, J., Kind, R., Sobolev, S. V., Kämpf, H., Wylegalla, K., Stiller, M., TOR Working Group, 1999. Major crustal features between the Harz Mountains and the Baltic Shield derived from receiver functions. Tectonophysics 314 (1–3), 321–333.

Grad, M., Janik, T., Yliniemi, J., Guterch, A., Luosto, U., Komminaho, K., Środa, P., Höing, K., Makris, J., Lund, C-E., 1999. Crustal structure of the Mid Polish Trough beneath TTZ seismic profile. Tectonophysics 314(1-3), 145–160.

Grad, M., Guterch, A., Mazur, S., 2002. Seismic refraction evidence for crustal structure in the central part of the Trans-European Suture Zone in Poland. In: Winchester, J.A., Pharaoh, T.C., Verniers, J. (Eds.), Palaeozoic Amalgamation of Central Europe. Geological Society of London Special Publications 201, pp. 295–309.

Grad, M., Jensen, S.L., Keller, G.R., Guterch, A., Thybo, H., Janik, T., Tiira, T., Yliniemi, J., Luosto, U., Motuza, G., Nasedkin, V., Czuba, W., Gaczyński, E., Środa, P., Miller, K.C., Wilde-Piórko, M., Komminaho, K.,

Jacyna, J., Korabliova, L., 2003. Crustal structure of the Trans-European suture zone region along POLONAISE'97 seismic profile P4. Journal of Geophysical Research, Solid Earth 108 (B11).

Guggisberg, B., Kaminski, W., Prodehl C., 1991. Crustal structure of the Fennoscandian Shield: A traveltime interpretation of the long-range FENNOLORA seismic refraction profile. Tectonophysrcs 195, 105–137.

Guterch, A., 1970. Kinematics and dynamics of seismic waves in selected heterogeneously stratified models of the continental Earth's crust. Publs. Inst. Geoph. PAS 39, PWN, Warszawa, 68 pp. + ill.

Guterch, A., Grad, M., 2006. Lithospheric structure of the TESZ in Poland based on modern seismic experiments. Geological Quarterly, 50, (1), 23–32.

Guterch, A., Grad, M., Janik, T., Materzok, R., Luosto, U., Yliniemi J., Lück, E., Schulze, A., Förste, K., 1994. Crustal structure of the transition zone between Precambrian and Variscan Europe from new seismic data along LT-7 profile (NW Poland and eastern Germany). C.R. Acad Sci. Paris 319, serie II, 1489–1496.

Guterch, A., Grad, M., Thybo, H., Keller, G.R., the POLONAISE Working Group, 1999. POLONAISE'97—an international seismic experiment between Precambrian and Variscan Europe in Poland. Tectonophysics 314 (1–3), 101–121.

Hübscher, C., Ahlrichs, H., Allum, G., Behrens, T., Bülow, J., Krawczyk, C., Damm, V., Demir, Ü., Engels, M., Frahm, L., Grzyb, G., Hahn, B., Heyde, I., Juhlin, C., Knevels, K., Lange, G., Bruun Lydersen, I., Malinowski, M., Noack, V., Preine, J., Rampersad, K., Schnabel, M., Seidel, E., Sopher, D., Stakemann, Jo., Stakemann, Ja., 2017. BalTec - Cruise No. MSM52 – March 1 – March 28, 2016 – Rostock (Germany) – Kiel (Germany). MARIA S. MERIAN-Berichte, MSM52, 46 pp., DFG-Senatskommission für Ozeanographie, DOI:10.2312/cr_msm52

Janik, T., Grad, M., Guterch, A., Dadlez, R., Yliniemi, J., Tiira, T., Keller, G. R., Gaczyński, E., CELEBRATION 2000 Working Group, 2005. Lithospheric structure of the Trans-European Suture Zone along the TTZ & CEL03 seismic profiles (from NW to SE Poland). Tectonophysics 411, 129–156.

Janik, T., Yliniemi, J., Grad, M., Thybo, H., Tiira, T., POLONAISE P2 Working Group, 2002. Crustal structure across the TESZ along POLONAISE'97 seismic profile P2 in NW Poland. Tectonophysics 360, 129–152.

Jaworowski, K., Wagner, R., Modlinski, Z., Pokorski, J., Sokołowski, A., Sokołowski, J., 2010. Marine ecogeology in semi-closed basin: case study on a threat of geogenic pollution of the southern Baltic Sea (Polish Exclusive Economic Zone). Geological Quarterly 54(2), 267–288.

Jóźwiak, W., 2013. Electromagnetic study of lithospheric structure in the marginal zone of East European Craton in NW Poland. Acta Geophysica 61(5), 1101–1129.

Katzung, G., Giese, U., Walter, R., Von Winterfeld, C., 1993. The Rügen Caledonides, northeast Germany. Geological Magazine 130 (5), 725–730.

Katzung, G., Giese, U., Maletz, J., Servais, T., Van Grootel, G., 1995. The eastern end of Avalonia: continuation into northern central Europe. In: Cooper, J.D., Droser, M.L., Finney, S.C. (Eds.), Ordovician Odyssey. The Pacific Section Society for Sedimentary Geology 77, pp. 233–236.

Krawczyk, C. M., Stiller, M., DEKORP-BASIN Research Group, 1999. Reflection seismic constraints on Paleozoic crustal structure and Moho beneath the NE German Basin. Tectonophysics 314, 241–253.

Krawczyk, C. M., Eilts, F., Lassen, A., Thybo, H., 2002. Seismic evidence of Caledonian deformed crust and uppermost mantle structures in the northern part of the Trans-European Suture Zone, SW Baltic Sea. Tectonophysics 360 (1), 215–244.

Komminaho, K., 1998. Software manual for programs MODEL and XRAYS: A graphical interface for SEIS83 program package, University of Oulu, Dep. of Geophys., Rep. 20, 31 pp.

Kramarska, R., Krzywiec, P., Dadlez, R., Jegliński, W., Papiernik, B., Przezdziecki, P., Zientara, P., 1999. Geological map of the Baltic Sea bottom without Quaternary deposits, 1: 500 000. Państwowy Instytut Geologiczny, Gdańsk-Warszawa.

Krzywiec, P., Kramarska, R., Zientara, P., 2003. Strike-slip tectonics within the SW Baltic Sea and its relationship to the inversion of the Mid-Polish Trough – evidence from high-resolution seismic data. Tectonophysics 373 (1-4), 93–105.

Krzywiec, P., Lis, P., Buffenmyer, V., Malinowski, M., Lewandowski, M., 2013. Regional geologic characterization of the Polish Lower Paleozoic unconventional play using an integrated seismic and well data approach. Unconventional Resources Technology Conference, Society of Exploration Geophysicists, American Association of Petroleum Geologists, Society of Petroleum Engineers 183–187.

Krzywiec, P., Kufrasa, M., Poprawa, P., Mazur, S., Koperska, M., Ślemp, P., 2021. Together but separate: decoupled Variscan (late Carboniferous) and Alpine (Late Cretaceous–Paleogene) inversion tectonics in NW Poland. Solid Earth Discussions 1–38.

Kubicki, S., 1984. Mineralization in the crystalline basement of North-Eastern Poland. Biuletyn Instytutu Geologicznego 347, 49–54.

Lassen, N.A., Thybo, H., Berthelsen, A., 2001. Reflection seismic evidence for Caledonian deformed sediments above Sveconorwegian basement in the southwestern Baltic Sea. Tectonics 20 (2), 268–276.

Liboriussen, J., Ashton, P., Tygesen, T. 1987. The tectonic evolution of the Fennoscandian Border Zone in Denmark. Tectonophysics 137, 21–29.

Ludwig, W.J., Nafe, J.E., Drake, C.L., 1970. Seismic refraction. In: Maxwell, A.E. (Ed.), The Sea, vol. 4, Wiley-Interscience, New York, pp. 53–84.

Luosto, U., 1997. Structure of the Earth's Crust in Fennoscandia as Revealed from Refraction and Wide-Angle Reflection Studies, Geophysica 33(1), 3–16.

Makris, J., Wang, S.-R., 1994. Crustal Structure at the Tornquist-Teisseyre zone in the Southern Baltic Sea. Zeitschrift fur Geologische Wissenschaften 22 (1/2), 47–54.

Maystrenko, Y., Bayer, U., Scheck-Wenderoth, M., 2005. The Glueckstadt Graben, a sedimentary record between the North and Baltic Sea in north Central Europe. Tectonophysics 397 (1-2), 113–126.

Maystrenko, Y., Bayer, U., Brink, H. J., Littke, R., 2008. The Central European basin system–an overview. In: Littke, R., Bayer, U., Gajewski, D., Nelskamp, S. (Eds.), Dynamics of complex intracontinental basins, pp. 16–34.

Maystrenko, Y.P., Scheck-Wenderoth, M., 2013. 3D lithosphere-scale density model of the central European Basin System and adjacent areas. Tectonophysics 601, 53–77.

Mazur S., Mikołajczak M., Krzywiec P., Malinowski M., Buffenmyer V., Lewandowski M., 2015. Is the Teisseyre-Tor nquist Zone an ancient plate boundary of Baltica? Tectonics 34 (12), 2465–2477.

Mazur, S., Mikolajczak, M., Krzywiec, P., Malinowski, M., Lewandowski, M. Buffenmyer, V., 2016. Pomeranian Caledonides, NW Poland–a collisional suture or thin-skinned fold-and-thrust belt?. Tectonophysics 692, 29–43.

Mazur, S., Porębski, S. J., Kędzior, A., Paszkowski, M., Podhalańska, T., Poprawa, P., 2018. Refined timing and kinematics for Baltica–Avalonia convergence based on the sedimentary record of a foreland basin. Terra Nova 30 (1), 8–16.

Mazur, S., Malinowski, M., Maystrenko, Y.P., Gągała, Ł., 2021. Pre-existing lithospheric weak zone and its impact on continental rifting–The Mid-Polish Trough, Central European Basin System. Global and Planetary Change 198, 103417.

McCann, T., 1996. Pre-Permian of the north-east German Basin. Geological Journal 31(2), 159–177.

Meissner, R., Krawczyk, C. M., 1999. Caledonian and Proterozoic terrane accretion in the South-West Baltic Sea. Tectonophysics 314 (1–3), 255–267.

Mikołajczak, M., Mazur, S., Gągała, Ł., 2019. Depth-to-basement for the East European Craton and Teisseyre-Tornquist Zone in Poland based on potential field data. International Journal of Earth Sciences 108 (2), 547–567.

Modliński, Z., Podhalańska, T., 2010. Outline of the lithology and depositional features of the lower Paleozoic strata in the Polish part of the Baltic region. Geological Quarterly 54 (2), 109–121.

Mogensen, T. E., 1994. Palaeozoic structural development along the Tornquist Zone, Kattegat area, Denmark. Tectonophysics 240 191–214.

Mona Lisa Working Group, 1997. MONA LISA – Deep seismic investigations of the lithosphere in the southeastern North Sea. Tectonophysics 269 (1-2), 1–19.

Naliboff, J., Buiter, S.J., 2015. Rift reactivation and migration during multiphase extension. Earth and Planetary Sciences Letters 421, 58–67.

Narkiewicz, M., Maksym, A., Malinowski, M., Grad, M., Guterch, A., Petecki, Z., Probulski, J., Janik, T., Majdański, M., Środa, P., Czuba, W., Gaczyński, E., Jankowski, L., 2015. Transcurrent nature of the Teisseyre–Tornquist Zone in Central Europe: results of the POLCRUST-01 deep reflection seismic profile. International Journal of Earth Sciences 104 (3), 775–796.

Narkiewicz, M., Petecki, Z., 2017. Basement structure of the Paleozoic Platform in Poland. Geological Quarterly 61 (2), 502–520.

Petecki, Z., 2002. Gravity and magnetic modelling along the seismic LT-7 profile. Przegląd Geologiczny 50, 630–633 (in Polish, English summary).

Petecki, Z., Rosowiecka, O., 2017. A new magnetic anomaly map of Poland and its contribution to the recognition of crystalline basement rocks. Geological Quarterly 61 (4), 934–945.

Pharaoh, T. C., 1999. Palaeozoic terranes and their lithospheric boundaries within the Trans-European suture zone (TESZ): a review. Tectonophysics 314, 17–41.

Piske, J., Rasch, H.-J., Neumann, E., Zagora, K., 1994. Geologischer Bau und Entwicklung des Präperms der Insel Rügen und des angrenzenden Seegebietes. Zeitschrift der Deutschen Gesellschaft 22 (1/2), 212–226.

Poprawa, P., 2006. Development of the Caledonian collision zone along the western margin of Baltica and its relation to the foreland basin. Prace Państwowego Instytutu Geologicznego 186, 189–214.

Poprawa, P., Šliaupa, S., Stephenson, R., Lazauskien, J., 1999. Late Vendian–Early Palaeozoic tectonic evolution of the Baltic Basin: regional tectonic implications from subsidence analysis. Tectonophysics 314 (1), 219–239.

Scheck, M., Bayer, U., 1999. Evolution of the Northeast German Basin – inferences from a 3D structural model and subsidence analysis. Tectonophysics 313, 145–169.

Scheck-Wenderoth, M., Lamarche, J., 2005. Crustal memory and basin evolution in the central European Basin System—new insights from a 3D structural model. Tectonophysics 397 (1-2), 143–165.

Schlüter, H.U., Jürgens, U., Binot, F., Best, G., 1998. The importance of geological structures as natural sources of potentially hazardous substances in the southern part of the Baltic Sea. Zeitschrift der Deutschen Geologischen Gesellschaft 44 (1), 26–32.

Seequent, 2021. https://www.seequent.com/products-solutions/geosoft-oasis-montaj/gm-sys/ - accessed 03/09/2021

Seidel, E., Meschede, M., Obst, K., (2018). The Wiek Fault System east of Rügen Island: origin, tectonic phases and its relationship to the Trans-European Suture Zone. In: Kilhams, B., Kukla, P. A., Mazur, S., McKie, T., Mijnlieff, H. F., van Ojik K. (Eds.), Mesozoic Resource Potential in the Southern Permian Basin. Geological Society, London, Special Publications 469, 59–82.

Smit, J., van Wees, J.-D., Cloetingh, S., 2016. The Thor suture zone: from subduction to intraplate basin setting. Geology 44, 707–710.

Smit, J., van Wees, J. D., Cloetingh, S., 2018. Early Carboniferous extension in East Avalonia: 350 My record of lithospheric memory. Marine and Petroleum Geology 92, 1010–1027.

Środa, P. and POLONAISE Working Group (Czuba W., Guterch A., Środa P., Grad M., Thybo H., Keller G.R., Miller K.C., Tiira T., Luosto U., Yliniemi J., Motuza G., Nasedkin V.), 1999. P and S wave velocity model of the southwestern margin of the Precambrian East European Craton, POLONAISE'97, profile P3. Tectonophysics 314(1-3), 175–192.

Talwani, M., Ewing, M., 1960. Rapid computation of gravitational attraction of three-dimensional bodies of arbitrary shape. Geophysics 25, 203–225.

Tanner, B., Meissner, R., 1996. Caledonian deformation upon southwest Baltica and its tectonic implications: alternatives and consequences. Tectonics 15 (4), 803–812.

Thybo, H., 1997. Geophysical characteristics of the Tornquist Fan area, northwest Trans-European Suture Zone: indication of the late Carboniferous to early Permian dextral transtension. Geological Magazine 134 (5), 597–606.

Thybo, H., 2000. Crustal structure and tectonic evolution of the Tornquist Fan region as revealed by geophysical methods. Bulletin of the Geological Society of Denmark 46, 145–160.

Thybo, H., 2001. Crustal structure along the EGT profile across the Tornquist Fan interpreted from seismic, gravity and magnetic data. Tectonophysics 334(3-4), 155–190.

Thybo, H., Abramovitz, T., Lassen, A., Schjøth, F., 1994. Deep structure of the Sorgenfrei-Tornquist zone interpreted from BABEL seismic data. Zeitschrift für Geologische Wissenschaften 22, 3–17.

van Wees, J. D., Stephenson, R. A., Ziegler, P. A., Bayer, U., McCann, T., Dadlez, R., Gaupp, R., Narkiewicz, M., Bitzer, F., Scheck, M., 2000. On the origin of the Southern Permian Basin, Central Europe. Marine and Petroleum Geology 17, 43–59.

Vecsey, L., Plomerová, J., Babuška, V., 2014. Mantle lithosphere transition from the East European Craton to the Variscan Bohemian Massif imaged by shear-wave splitting. Solid Earth 5(2), 779–792.

Vejbæk, O. V., 1997. Dybe strukturer i danske bassiner. Geologisk Tidsskrift 4, 1–31.

Vejbæk, O. V., Stouge, S., Poulsen, K. D., 1994. Palaeozoic tectonic and sedimentary evolution and hydrocarbon prospectivity in the Bomholm area. Danmarks Geologiske Undersøgelse, A34, 1–23.

Wessel, P., Smith, W.H.F., 1995. New version of the Generic Mapping Tools released. EOS Transactions of the American Geophysical Union 76, 329.

Wilde-Piórko, M., Geissler, W.H., Plomerova, J., Grad, M., Babuska, V., Bruckl, E., Cyziene, J., Czuba, W., England, R., Gaczyński, E., Gazdova, R., Gregersen, S., Guterch, A., Hanka, W., Hegedus, E., Heuer, B., Jedlicka, P., Lazuskiene, J., Keller, G.R., Kind, R., Klinge, K., Kolinsky, P., Komminaho, K., Kozlovskaya, E., Kruger, F., Larsen, T., Majdański, M., Malek, J., Motuza, G., Novotny, O., Pietrasiak, R., Plenefisch, Th., Ruzrk, B., Sliaupa, S., Środa, P., Świeczak, M., Tiira, T., Voss, P. and Wiejacz, P., 2008. PASSEQ 2006-2008: Passive Seismic Experiment in Trans-European Suture Zone. Studia Geophysica et Geodetica 52, 439-448.

Yang, H., Chemia, Z., Artemieva, I.M., Thybo, H., 2018. Control on off-rift magmatism: a case study of the Baikal Rift Zone. Earth and Planetary Sciences Letters 482, 501–509.

Zelt, C.A., 1994. Software Package ZPLOT. Bullard Laboratories, University of Cambridge.

Zeyen, H., Volker, F., Wehrle, V., Fuchs, K., Sobolev, S.V., Altherr, R., 1997. Styles of continental rifting: crust-mantle detachment and mantle plumes. Tectonophysics 278 (1-4), 329–352.